OBSERVATIONS OF NEUTRAL V-PARTICLE DECAYS

WITH THE 48" MAGNET CLOUD CHAMBERS

Thesis by

Victor A. J. van Lint

In Partial Fulfillment of the Requirements

for the Degree of

Doctor of Philosophy

California Institute of Technology

Pasadena, California

1954

ACKNOWLEDGEMENTS

niques for analyzing V-particles which nevertheless retains the precision inherent in the photographs.

Foremost among the many graduate students who worked with the author was Mr. George H. Trilling. He joined the project at its beginning and has contributed greatly to the construction and operation of the equipment and the analysis of the data. He has also participated in many fruitful discussions concerning improvements to the equipment, interpretation of the data, and many other problems in physics.

Other graduate students who contributed greatly to the construction work and the operation of the equipment include Mr. Carl A. Rouse and Mr. Arnold A. Strassenburg. Their assistance with the operation of the equipment enabled the author to spend much of his time analyzing the data.

Dr. R. V. Adams assisted the project during the summer of 1953 by analyzing many V-particle photographs. His contribution to the results through discussions of improvements in the measurement technique and interpretation of the data was also extremely valuable.

No large construction job can be undertaken efficiently without the assistance of capable draftsmen and machinists. Mr. R. B. Pollock made most of the design drawings and supervised many of the machining operations. The author is particularly indebted to Mr. P. F. Fuselier, whose advice on machine shop practice and contribution to

some of the precision machining work was invaluable. It
is, of course, not possible to name the many others who
participated in the construction work and thus helped to
make the project a success, but their contributions are
greatly appreciated.

ABSTRACT

This thesis is the first to result from operation of
the 48" magnet cloud chambers at the California Institute
of Technology. The apparatus is not described here in any
detail. The techniques used to measure track curvatures
and the positions of points inside the chambers are discussed
in detail as is the analysis of the possible errors in these
quantities. A formula is derived for computing the momentum
of a particle from its measured curvature on the film. It
includes corrections for the nonaxial components of the
magnetic field and the effect of the conical projection
involved in the photography. A method for correcting ap-
proximately for the variation of the magnetic field along
the track is also presented.

A summary of the dynamics of the two-body decay of a
neutral V-particle is presented. A discussion of the uses
of plots of α and P_T for a two-body decay is included.
The dynamics of some simple three-body decays are discussed.
The distribution of the momenta of one of the decay pro-
ducts is derived, including only the effects of the den-
sity of states in phase space. An attempt is made to analyze
the observable properties of a three-body decay when the two
charged products are treated as products of a two-body
decay.

The results from the analysis of the best cases of Λ^O
and θ^O decays observed in the 48" magnet cloud chambers
are summarized. They include a value for the energy re-
lease in the Λ^O decay of (34.8 ± 1) Mev, and a preliminary
discussion of the coplanarity and transverse momentum
balance for those cases in which an origin for the V^O-
particle can be located. In addition, an excellent case
of the decay of a neutral V-particle into two light secon-
daries with an energy release much lower than that for
the usual θ^O decay scheme forms the basis for the discus-
sion of all such "anomalous θ^O" decays observed in the
three Caltech magnet cloud chambers.

CONTENTS

FIGURES

I. EXPERIMENTAL TECHNIQUE

A. Apparatus

The 48" magnet has an air gap which measures 46"
high, 24" wide, and 12" deep. The magnetic field in the
air gap averages about 8000 gauss and is produced by a
direct current of 800 amperes at 110 volts. The magnet
is water cooled and is provided with safety circuits
which de-energize it in case of a failure in the cooling
system. Fig. 1 is a photograph looking down on the magnet,
also showing the rack of electronic chamber control circuits.

The cloud chambers are similar in design, but larger
in scale, to the 18" magnet cloud chambers which were de-
signed and operated by Dr. R. B. Leighton. They are rigid-
piston, rectangular body, expansion-type chambers with an
illuminated volume measuring 22" wide, 8" high, and 8" deep.
The tracks are photographed through a plate glass front
window against a background of black velvet fastened to the
piston. The other inner surfaces are polished and chromium
plated except for an illumination window in one side. The
geometry of the chambers, geiger counters, absorbers, and
cameras is shown in Fig. 2. Four chambers, each above
an other, were used until July 1953, at which time the
upper two chambers were replaced by one double-height
chamber.

The cloud chambers, as well as the air and metal
surfaces touching them, are held at an accurately con-
trolled temperature by passing water through copper tubes

Fig. 1. Cosmic Ray Laboratory

This photograph of the cosmic ray laboratory shows the 48" magnet from above. The iron flux return path can be seen in the bottom foreground. The rear current coils and cooling jackets are barely visible at the right edge of the photograph. The lead blocks above the chambers can just be seen in the open thermostat box at the right. The magnet cooling water exhaust manifolds are in the foreground. The electronic control circuits are shown at the left edge. The cameras are in the box which protrudes from the side of the magnet facing the electronics rack.
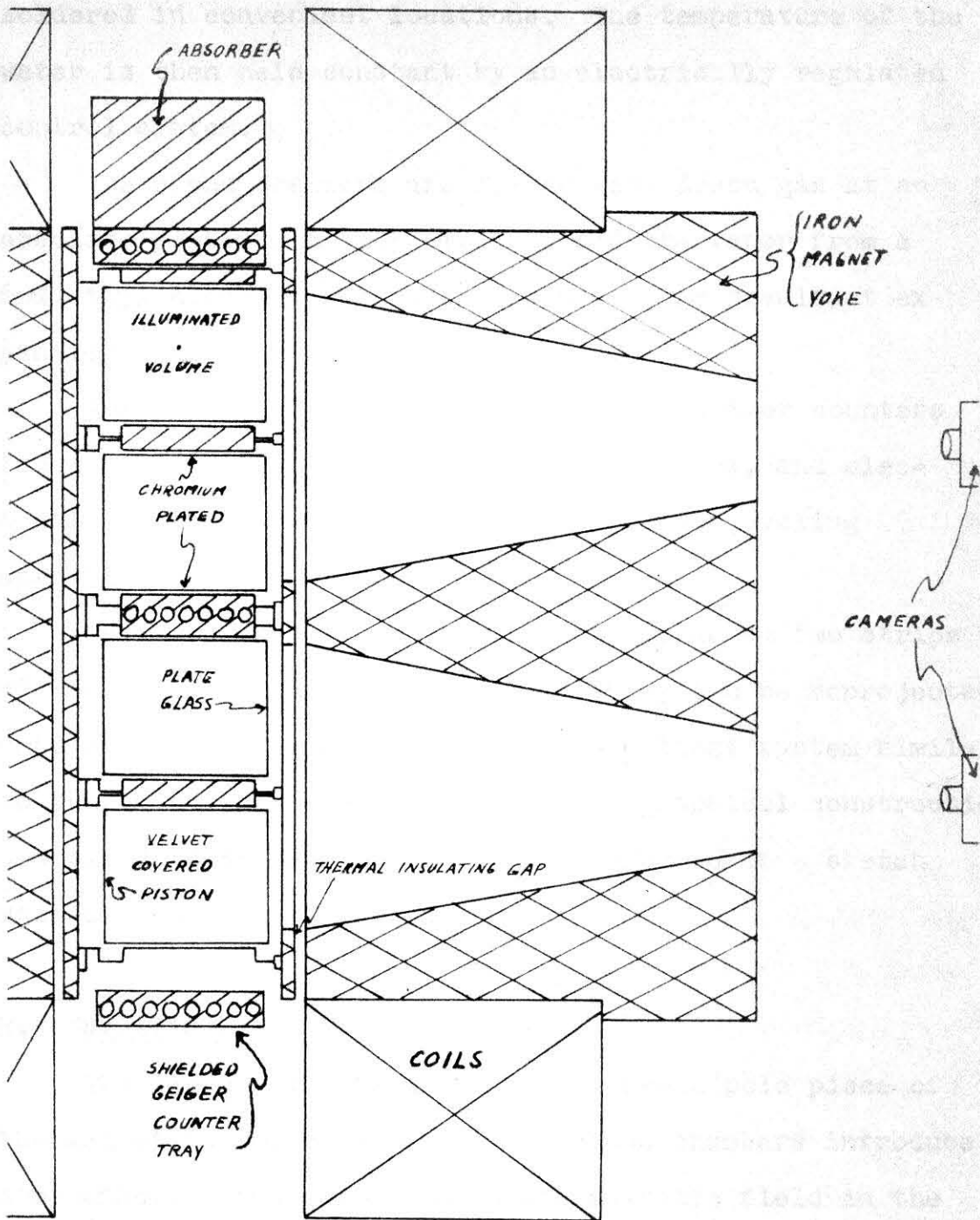
Fig. 2. Chamber Geometry

In July 1953 the top two cloud chambers were re-
placed by a single double-height chamber.

soldered in convenient locations. The temperature of the water is then held constant by an electrically regulated control system.

The cloud chambers are filled with Argon gas at an absolute pressure of 105 cm. Hg., and the vapor from a 60% ethyl alcohol, 40% water mixture. The resultant expansion ratio was usually near 1.075.

The entire operation is automatic. Geiger counters function as detectors of penetrating showers, and electronic control systems initiate the various cycling operations.

The stereoscopic photographs are taken on two strips of 70mm. Kodak Linagraph Pan film. They can be reprojected onto a plane at full size through an optical system similar to that used in the photography. The graphical constructions described in Section I-D are then performed on a sketch made of the projected views.

B. Magnetic Field Measurement

The large holes required in the front pole piece of the magnet for observation of the cloud chambers introduce appreciable nonuniformities in the magnetic field in the air gap. In addition, the depth of the air gap is comparable to its width so that there is appreciable bulging of the lines of magnetic flux. In order to make accurate measurements of the momentum of a cosmic ray track it is

necessary to know the value, as well as the direction, of
the magnetic induction along the track. Measurements were
carried out to determine B_Z (the component of B normal to
the pole faces) and the component ratios, $p = \frac{B_x}{B_z}$, $q = \frac{B_y}{B_z}$.
(The X direction is horizontal, the Y direction vertical,
so as to form a right handed co-ordinate system with the
Z co-ordinate increasing toward the camera).

The normal component, B_Z, was measured using a flip
coil and a G. E. Model 248 Fluxmeter. The flip coil was
constructed of one turn of Formvar coated copper wire
wound around a 3/4" diameter bakelite disk, which was con-
nected to a bakelite handle by means of a hollow cylindri-
cal bearing. The leads from the coil were twisted and led
through the bearing and along the handle. The coil was
flipped by a coil spring around the bearing upon the re-
lease of a trigger. This design was adopted to avoid
errors caused by the flux that is cut by the leads when
a rigid coil assembly is flipped as a unit. The absolute
value of the magnetic field was determined at a standard
(X,Y) location for various Z co-ordinates in the gap by
comparing the fluxmeter deflection with that when the
coil was flipped in a standard permanent magnet. This
magnet was in turn checked against a proton resonance fre-
quency controlled magnet using the same fluxmeter and the
same flip coil. The probable error in the determination
of the absolute value of the magnetic field is less than

±50 gauss. Furthermore, the difference between B_Z at various (X,Y) co-ordinates and that at the standard (X,Y) location for the same Z depth was measured using a coil of many turns and correspondingly higher accuracy. Therefore, accurate, repeated fluxmeter readings needed to be taken for only the few absolute measurements.

The component ratios, p and q, were measured using a brass holder which supported a steel needle freely at its center. A small piece of graph paper was mounted parallel to the bottom surface of the holder so that the deflection of the needle from a perpendicular position can be determined by reading the X and Y co-ordinates subtended by the end of the needle on the graph paper.

The values of B_Z, p, and q were then plotted in the form of contour maps for the planes Z=1, 11, 16, and 21 cm. (The Z=0 plane is the plane of the front surface of the chamber piston in the compressed position). The extra plane between the center and the front was measured because the hole in the front pole piece causes the field to change rapidly in this region. The contour interval and the distances between planes were chosen so that linear interpolations would not make errors of greater then $\frac{1}{2}\%$. Since the uncertainty in the momentum of a single track due to multiple scattering in the Argon gas used in the chambers is never less than about 2%, the error in determination of the magnetic field is usually negligible. However, it was

found that it is necessary to keep the temperature of the
magnet coils reasonably constant since an increase in the
average cooling water temperature from 35°C to 60°C produced
magnetic field changes due to redistribution of current in
the coils of the order of 3%.

C. Curvature Measurement

In using the momentum calculation formula derived in
Section II, the quantity which characterizes the apparent
curvature of the track is the sagitta at the center of the
conically projected track. Therefore, it is necessary to
measure the location of the track at three points only.
However, in order to check on convection distortions or
to detect a possible single scattering along the track, it
is convenient to check that the track is circular within
the perturbations introduced due to a changing magnetic
field and the δ_2 correction (see Section II). The follow-
ing techniques have been used for measuring the curvature
of tracks.

The most accurate technique is to determine co-ordinates
of points on the track using a precision comparator and
to plot these co-ordinates on graph paper, magnifying trans-
verse dimensions by a factor of 10 or 20 times more than
the longitudinal dimensions. The resulting elliptical track
can be approximated closely by standard parabolas. The
sagitta of the track can also be measured.

This procedure is time consuming and is difficult
to apply when faint tracks are involved, since some con-
trast is lost in the optical system of the comparator
microscope. Extreme caution must also be taken not to
emphasize large clusters of droplets which appear along
the track, since these are often due to low energy delta
rays which might have been ejected over to one side of
the main track. In order to avoid these difficulties,
Dr. Leighton designed and constructed an instrument which
mechanically magnifies the lateral dimension by about 10
times. It consists of two round aluminum rails on which
a carriage rides. On this carriage a fine pointer and a
pencil, provided with ways for lateral motion, are driven
by wires. Each wire passes over one of two pulleys which
are coupled together and whose diameters differ by a factor
of about 10. In this manner the pencil is constrained to
move at a rate about 10 times that of the pointer. By fol-
lowing a track accurately with the pointer, the pencil
traces the corresponding laterally magnified image. By
going over the track a number of times in both directions,
small random errors in setting the pointer on the track
are cancelled out. It is also possible to sight carefully
along the track to enable one to see a faint image. The
resulting plot is then used similarly to a comparator plot:
namely, the consistency of the plot with a parabola is
checked and the sagitta measured. Possible sources of error

in this method lie in the subjective nature of the track
following procedure and the reliance upon the linearity
of the reprojection system.

Another still faster technique is to compare the
track directly with circles scribed on lucite sheets.
Since a solid line on the sheet obscures the track be-
neath it, it is convenient to have two comparison circles
of the same radius separated by a distance slightly greater
than a track width. This method is not as accurate nor
as objective as the previously described methods but
does take much less time. It can therefore be profitably
used on noncritical curvature measurements.

When the track is extremely curved and has a large
sagitta, it may be sufficient to make a direct measurement
of the sagitta, without any artificial magnification, using
a straight-edge and an accurate scale. This method is
perhaps less subjective than a comparison with circles
and the result may correspond more closely to the desired
sagitta measurement, but it overemphasizes very short
sections of the track.

D. Co-ordinate Measurement

The positions of pertinent points in the cloud cham-
ber are determined from a full-size reprojection of the
stereoscopic photographs. The two conically projected
views, hereafter called apparent views, are projected

onto a horizontal plate glass on which a sheet of vellum is placed. The two apparent views of fiducial marks on the front surface of the chamber piston are accurately superimposed and the separation between marks normalized to full size by adjusting the projector magnification. Many adjustments are needed on the projector to make the superposition very accurate over the whole extent of the piston.

Once the images of the piston are in coincidence, the Z co-ordinate of any point in space (corrected for the expansion of the chamber) can be calculated from the horizontal separation between the two apparent views of the point. Thus $Z = \frac{1}{1+\varepsilon} \frac{D\delta X}{S+\delta X}$, where D is the distance from the front surface of the piston to the front principal plane of the lens (D = 125 cm. for the 48" magnet cloud chambers); S is the separation between the camera lenses (S = 17.8 cm.); $1 + \varepsilon$ is the expansion ratio ($\varepsilon \sim .075$); and δX is the measured horizontal separation.

In order to measure the other co-ordinates, X and Y, of a point, it is convenient to construct the orthogonal projection of the point on the piston surface. This is done from the sketched apparent views as shown in Fig. 3. The apparent views of a point (A_L, A_R) and the corresponding lens axes (L_L, L_R) are joined by straight lines. Each of these lines is the orthogonal projection of a line
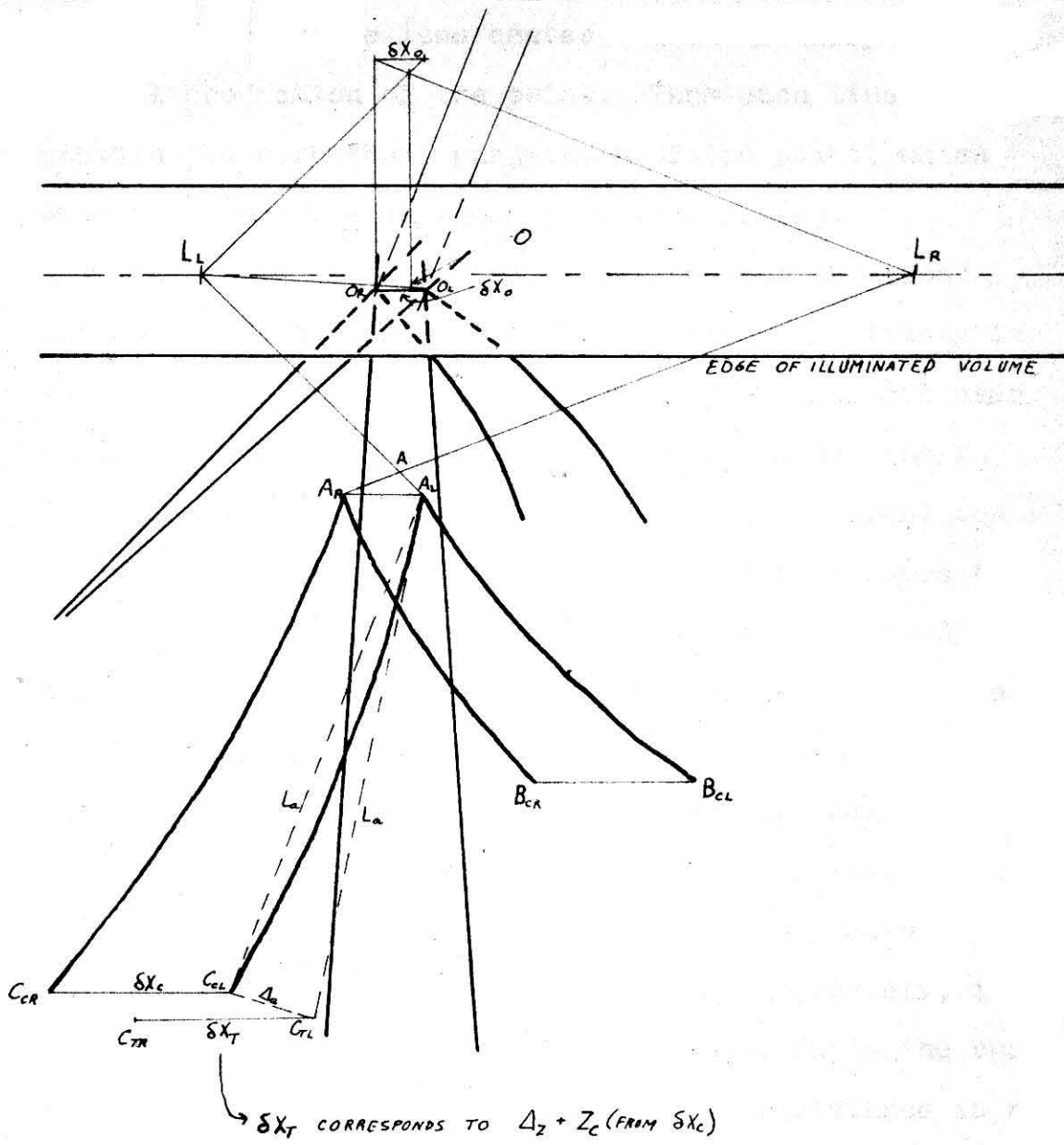
Fig. 3. Graphical Constructions

This figure demonstrates the graphical constructions applied to the analysis of a V^O decay event. The construction of the orthogonal view is described in Section I-D; the construction of the tangent to the track in Section II-G.

passing through the lens center and the corresponding

conical projection of the point. Thus each line must

contain the orthogonal projection of the point, which

must therefore lie at their intersection (A).

It should be noted that the above construction

introduces a large possible construction uncertainty in

the X co-ordinate if the point has a Y co-ordinate near

zero; e. g. point O of Fig. 3. However, since the X

co-ordinate is related to a given pair of apparent co-

ordinates, X_{aL} and X_{aR}, independently of Y, a correct

procedure is to reproduce the interval δX at some distance

directly below or above O_L-O_R. Then the X co-ordinate

can be reprojected back to the original Y distance after it

has been determined by the prescribed graphical procedure.

When locating a possible origin for a V-particle it

is necessary to extrapolate tracks into the regions beyond

the chambers. In order to do this most accurately, it is

desirable to continue the curvature measured in the cham-

ber along the extrapolation, provided the distance is not

so great that the magnetic field has decreased appreciably.

To do this quickly a rough measurement of the radius of

curvature is made using standard circular arcs scribed

on sheets of lucite. The circular arc is then allowed to

extend slightly beyond the track and a mark is made at

the end of the arc. This procedure is continued, locating

a number of points on the extrapolation, thus extending it

as far as is needed. The extrapolated curve is then approx-
imated by straight line segments drawn between the construc-
ted points, and the curve in the chamber is sketched. Often,
when the tracks are almost straight, only one point near
the location of the origin has to be constructed. After
having extrapolated many tracks one should weight the
straightest ones most heavily in deciding the exact loca-
tion of the origin because errors due to multiple scatter-
ing of the particles in the solid material have less effect
on particles of large $P\beta$. Using the above constructions,
and the method for constructing tangents to tracks derived
in Section II-G and illustrated in Fig. 3, it is possible
to measure ΔX, ΔY, and ΔZ for all pertinent lines. We thus
have available all the data needed to compute the momenta
of the tracks as well as the angles between them.

The angles can be computed using the scalar product
of the vectors: $\cos\theta_{12} = \dfrac{\Delta X_1 \Delta X_2 + \Delta Y_1 \Delta Y_2 + \Delta Z_1 \Delta Z_2}{L_1 L_2}$. How-
ever, when θ_{12} is small, the cosine is a very slowly
varying function. Since it is desirable to use a slide
rule for these computations, the following formula is
more satisfactory for small angles:
$$2\sin^2\theta_{12}/2 = 1 - \cos\theta_{12} = \frac{L_{12}{}^2 - (L_1 - L_2)^2}{2L_1 L_2}$$, where L_{12} is
the distance between the end points of L_1 and L_2. It is
often convenient to renormalize co-ordinates so that
$L_1 = L_2$.

An important quantity to calculate for many V^o decay

events is the coplanarity angle, "δ". This is the angle
between the line of flight of the neutral primary and the
plane defined by the tangents to the lines of flight of
the secondaries at the apex. It can be computed from the
vectors by using the formula

$$\sin\delta = \frac{\vec{L}_0 \cdot \vec{L}_+ x \vec{L}_-}{L_0 L_+ L_- \sin\theta_{+-}} \quad .$$

However, the evaluation of the determinant which is
involved in calculating the numerator is a tedious pro-
cedure. If the angles θ_{+0}, θ_{0-}, and θ_{+-} have been calcu-
lated accurately, the following formula, which can be derived
from the corresponding spherical triangle relations, can be
used:

$$\sin^2\delta = \frac{4\sin\Delta/2\sin(\theta_{+-}+\Delta/2)\sin(\theta_{+0}-\Delta/2)\sin(\theta_{0-}-\Delta/2)}{\sin^2\theta_{+-}}$$

where $\quad \Delta = \theta_{+0} + \theta_{0-} - \theta_{+-}$

Only when there is a long primary path and an accurately
located origin for the V^0-particle is the above formula,
together with slide rule accuracy, not sufficient. Then
the determinant form should be calculated using great
care to avoid subtracting large, but almost equal, numbers.

E. Estimation of Errors

The important errors in the calculated results on
V-particle decays can come from the following sources:

    1. convection current distortions in curvatures

    2. measurement errors in curvatures

3. lens and film distortion in curvatures

4. magnetic field calibration errors

5. errors in the measurement of the positions of points in the chamber

6. errors in extrapolation of tracks to an interaction

7. *errors in estimating specific ionizations*

8. possible errors in other parameters

The effects of each of these errors will now be estimated.

1. *The most important error in the measurements per-*formed to date has been due to the convection currents in the cloud chamber gas prior to the expansion. Unfortunately, it has not been possible to make a systematic quantitative analysis of the distortions by taking pictures with no magnetic field, for two reasons. Firstly, there are some leaks in the magnet cooling jackets which are aggravated by repeatedly turning the magnet on and off. The cause lies in the slight motions of the conductors and cooling jackets due to the changing magnetic forces. Secondly, the thermostat system has undergone numerous changes during the first year of operation and the temperature conditions have varied greatly. Thus any quantitative analysis would have to have been done many times with different results each time.

For these reasons, the estimated errors have been assigned more or less subjectively. This procedure is not unreasonable since there are certain clear evidences of the presence of convection distortions. Experience with

similar geometry in the 18" magnet cloud chambers, as well as the 48" chambers, has indicated that slight kinks near the chamber walls invariably precede any large scale distortions. Furthermore, primaries of very energetic interactions can be checked for straightness, and the curvatures of a single track above and below an absorber plate can be measured and compared. During most of the time the data described in this thesis were taken, the maximum detectable momentum for a 20 cm. long track was estimated to be about 3 Bev/c. When in doubt, conservativeness prevailed and larger errors were assigned.

2. Errors in measurement of curvatures played no essential part in the data presented in this thesis. The convection current distortions were always appreciably larger whenever the curvatures were measured by the comparator method.

3. Lens and film distortion played no important part in these measurements. They have not appeared on the film to any recognizable degree. The only indications of photographic distortions have appeared when reprojecting with the lenses opened up to f/4. Then the curvatures measured with Dr. Leighton's plotter are sometimes misleading due to either a lens distortion or a misjudgement in the location of the image caused by the excess light. For the first ten months of operation there was also a slight effect due to buckling of the film. Flat pressure

plates were installed in the cameras to eliminate such
difficulties. A slight suction applied to holes in the
pressure plate forces the film to lie against the flat
surface.

4. The main error in calibrating the magnetic field
is due to the fact that the standard permanent magnet has
a magnetic induction of only 2300 gauss or about 2/7 that
of the large magnet. Thus the reading of the fluxmeter
when the coil is flipped in the standard field has to be
taken repeatedly and very carefully to avoid a large per-
centage error. It is estimated that due to this cause,
the absolute value of the magnetic induction is uncertain
by a probable error of ±50 gauss. On an individual meas-
urement of a momentum this corresponds to an error of about
±.7%, and is therefore negligible compared to multiple
scattering errors. However, this magnetic field error
is systematic and can contribute a slight additional
error to a statistically averaged number: e. g. the aver-
age Q-value from a number of similar V-particle decay
events.

Errors in the component ratios, p and q, are negli-
gible in all cases. The uncertainty is about ±.01, but
the errors are statistical and the component ratios enter
into the momentum only when multiplied by Z_0', which is
usually less than .5.

5. The main error in location of points in the cham-

ber arises from the Z depth measurement. Using the best
techniques available with the existing projectors, the
estimated error in measurement of the horizontal separa-
tion between the two apparent views of a point is ±.016 cm.
This corresponds to an uncertainty in Z depth of ±.1 cm.
For tracks which lie near the XY plane the measurements
of angles depend mostly on errors in ΔX and ΔY, which can
be measured to ±.03 cm. In the cases of the V^O-particle
decays that have been analyzed, the errors in angle measure-
ments contributed negligibly to the Q-value, but were some-
times important for transverse momentum balance and co-
planarity calculations.

6. Usually the most uncertain point used in a trans-
verse momentum balance or coplanarity calculation is the
origin of the V^O-particle. The accuracy of location of
the origin must be judged independently for each case from
the following factors:

a) the number of particles extrapolated

b) the length of the extrapolation

c) the curvatures of the tracks involved

d) possible multiple scattering errors

e) the average value of $Z_O{}'$ for the extrapolated
   tracks (X and Y co-ordinates can be measured
   about six times more accurately than Z co-
   ordinates on extrapolated tracks).

7. Since the technique of operation of the 48"
magnet cloud chambers has not yet been developed to the
stage where the individual droplets can be resolved on

the photographs, the specific ionizations have to be estimated visually. Naturally large errors are assigned to these estimates, usually corresponding to a factor of two between the extreme values allowed. However, in the data analysis that has been done to date, the ionization estimates have only been used to distinguish between protons and π-mesons; namely, to decide whether a particular V^O decay was a Λ^O decay or a θ^O decay. Having made such a decision, or having decided such a decision was uncertain, the Q-value was calculated assuming the secondaries to be $P^+ + \pi^-$ or $\pi^+ + \pi^-$.

8. A few of the other geometrical parameters which enter into the measurement of positions and calculation of momenta are: D, the distance from the front surface of the chamber piston to the front principal plane of the camera lens; S, the separation between the camera lenses; and also the distance between the fiducial marks on the piston which are used to normalize the magnification of the re-projection. These quantities have been carefully checked, either directly or by indirect experiments (e. g. the calculation of the Z co-ordinate of the back surface of the front glass from a measurement of the horizontal separation between the two apparent views of a dust speck). Thus these parameters are known accurately enough that they do not contribute any significant errors.

II. MOMENTUM CALCULATION

A. Formulation of the Problem

In the calculation of the momentum of an ionizing particle traversing a cloud chamber in a magnetic field, a number of corrections need to be made. Firstly, the magnetic field is in general neither uniform nor directed parallel to the camera axis. Secondly, in order to measure the curvature of the track it is not convenient to make an orthogonal projection of the track on any plane. The photograph, or a reprojection thereof, represents a conical projection of the track through the center of the camera lens onto a convenient plane. The purpose of the following calculation is to make an analysis of the resulting track.

We set up the following co-ordinate system in space: the Z axis is perpendicular to the rear cloud chamber wall and coincides with the lens axis. The XY plane coincides with the rear chamber wall; the Y axis is vertical and the X axis horizontal so as to form a right-handed co-ordinate system with the Z co-ordinate increasing toward the camera.

The position of the track in the chamber will be specified by the co-ordinates of a reference point on the track near its center, (X_0, Y_0, Z_0), and the direction cosines of the track at this point, (X_0', Y_0', Z_0'). The magnetic field will be specified by its Z component, B_Z,

and the component ratios, $p = \frac{B_x}{B_z}$ and $q = \frac{B_y}{B_z}$. The momentum, P, of the particle which produced the track will enter into the calculation only through the quantity $a = \frac{eB_z}{P}$. We shall solve the equations of the path parametrically using as the independent parameter, s, the distance along the track from the reference point.

B. Exact Equation of the Track in Space in A Uniform Magnetic Field

Let us first assume the magnetic field to be uniform in magnitude and direction along the track. The differential equations of the track are then

$$X'' = a(Y' - qZ')$$
$$Y'' = -a(X' - pZ')$$
$$Z'' = a(qX' - pY')$$

where the prime denotes differentiation with respect to s. These can be integrated once immediately to give

$$X' - X_0' = a[(Y - Y_0) - q(Z - Z_0)]$$
$$Y' - Y_0' = -a[(X - X_0) - p(Z - Z_0)]$$
$$Z' - Z_0' = a[q(X - X_0) - p(Y - Y_0)]$$

In order to solve these easily let us make the substitution

$$\xi = (X - X_0) - p(Z - Z_0)$$
$$\eta = (Y - Y_0) - q(Z - Z_0)$$
$$\zeta = Z - Z_0$$

The equations then become

$$\xi' + p\zeta' = \alpha\eta + X_0'$$
$$\eta' + q\zeta' = -\alpha\xi + Y_0'$$
$$\zeta' = \alpha(q\xi - p\eta) + Z_0'$$

from which ζ' can be eliminated. The resulting equations in ξ, η, ξ', η' can be solved by assuming a solution of the form $\xi = A\exp(i\alpha\beta s)$, $\eta = B\exp(i\alpha\beta s)$ as a homogeneous solution and adding constants as particular solutions. The secular determinant of the equations determines the two possible values of β to be $\pm\sqrt{1+p^2+q^2}$. The equations and the initial conditions determine all the constants, and the equation for ζ can be integrated directly. The solution is

$$\xi = \frac{1}{\alpha\beta^2}[pqX_0'-(1+p^2)Y_0'+qZ_0'][\cos(\alpha\beta s)-1] + \frac{1}{\alpha\beta}(X_0'-pZ_0')\sin(\alpha\beta s)$$

$$\eta = \frac{1}{\alpha\beta^2}[(1+q^2)X_0'-pqY_0'-pZ_0'][\cos(\alpha\beta s)-1] + \frac{1}{\alpha\beta}(Y_0'-qZ_0')\sin(\alpha\beta s)$$

$$\zeta = Z_0's + \frac{1}{\alpha\beta^2}(-qX_0'+pY_0')[\cos(\alpha\beta s)-1] - \frac{1}{\alpha\beta^3}[pX_0'+qY_0'-(p^2+q^2)Z_0'][\sin(\alpha\beta s)-(\alpha\beta s)]$$

Changing back to the original co-ordinates this becomes

$$X = X_0 + \frac{1}{\alpha\beta^2}(Y_0'-qZ_0')[1-\cos(\alpha\beta s)] + \frac{p}{\beta^2}(PX_0'+qY_0'+Z_0')s + \frac{1}{\alpha\beta^3}[(1+q^2)X_0'-pqY_0'-pZ_0']\sin(\alpha\beta s)$$

$$Y = Y_0 - \frac{1}{\alpha\beta^2}(X_0'-pZ_0')[1-\cos(\alpha\beta s)] + \frac{q}{\beta^2}(pX_0'+qY_0'+Z_0')s + \frac{1}{\alpha\beta^3}[-pqX_0'+(1+p^2)Y_0'-qZ_0']\sin(\alpha\beta s)$$

$$Z = Z_0 + \frac{1}{\alpha\beta^2}(qX_0'-pY_0')[1-\cos(\alpha\beta s)] + Z_0's + \frac{1}{\alpha\beta^3}[pX_0'+qY_0'-(p^2+q^2)Z_0'][(\alpha\beta s)-\sin(\alpha\beta s)]$$

At this point the only approximation that has been made is that the magnetic field is uniform. This is the exact parametric equation of the helical track in space referred to convenient co-ordinate axes.

C. Projection of the Track on the Rear Chamber Wall

In order to reduce to a useful form the equation we have derived we now perform two operations. Firstly, we must make a conical projection of this curve through the center of the lens $(0,0,D)$ onto the plane $Z=0$. This projection is the curve that is usually observed in an actual cloud chamber photograph. Secondly, since the parameter s has no direct significance on the projection, we shall transform to the parameter s_a, which is the arc length measured on the projection.

In general we can consider a track segment whose length is shorter than its radius. Thus, in order to make our formulas manageable, we shall expand them in powers of αs or αs_a. The convergence is very rapid, as will be seen by noting the magnitude of the correction terms which we shall derive.

Thus the parametric equations of the track in space become the following:

$$X = X_0 + X_0's + \tfrac{1}{2}a(Y_0'-qZ_0')s^2 - \tfrac{1}{6}a^2[(1+q^2)X_0'-pqY_0'-pZ_0']s^3$$

$$- \tfrac{1}{24}a^3\beta^2(Y_0'-qZ_0')s^4 + \ldots$$

$$Y = Y_0 + Y_0's - \tfrac{1}{2}a(X_0'-pZ_0')s^2 - \tfrac{1}{6}a^2[-pqX_0'+(1+p^2)Y_0'-qZ_0']s^3$$

$$+ \tfrac{1}{24}a^3\beta^2(X_0'-pZ_0')s^4 + \ldots$$

$$Z = Z_0 + Z_0's + \tfrac{1}{2}a(qX_0'-pY_0')s^2 + \tfrac{1}{6}a^2[pX_0'+qY_0'-(p^2+q^2)Z_0']s^5$$

$$- \tfrac{1}{24}a^3\beta^2(qX_0'-pY_0')s^4 + \ldots$$

Performing the indicated conical projection and defining

co-ordinates on that projection as (X_a,Y_a) we get,

$$X_a = X\frac{D}{D-Z} \quad ; \quad Y_a = Y\frac{D}{D-Z} \quad ; \quad \text{Define} \quad \gamma = \frac{D}{D-Z_0}$$

Then
$$X_a = X_{ao}+X_{ao}'s+\tfrac{1}{2}X_{ao}''s^2+\tfrac{1}{6}X_{ao}'''s^3+\tfrac{1}{24}X_{ao}^{(iv)}s^4+\ldots$$

$$Y_a = Y_{ao}+Y_{ao}'s+\tfrac{1}{2}Y_{ao}''s^2+\tfrac{1}{6}Y_{ao}'''s^3+\tfrac{1}{24}Y_{ao}^{(iv)}s^4+\ldots$$

where $X_{ao} = \gamma X_0$ $\qquad\qquad Y_{ao} = \gamma Y_0$

$$X_{ao}' = \gamma\left(X_0'+\frac{X_0 Z_0'}{D}\right) \qquad\qquad Y_{ao}' = \gamma\left(Y_0'+\frac{Y_0 Z_0'}{D}\right)$$

$$X_{ao}'' = a\gamma\left\{Y_0'+\frac{2\gamma X_0'Z_0'}{aD}-qZ_0'+\frac{2\gamma^2 X_0 Z_0'^2}{aD^2}+\frac{\gamma X_0}{D}(qX_0'-pY_0')\right\}$$

$$Y_{ao}'' = -a\gamma\left\{X_0'-\frac{2\gamma Y_0'Z_0'}{aD}-pZ_0'-\frac{2\gamma^2 Y_0 Z_0'^2}{aD^2}-\frac{\gamma Y_0}{D}(qX_0'-pY_0')\right\}$$

$$X_{ao}''' = -a^2\gamma\left[X_0'-\frac{3\gamma Y_0'Z_0'}{aD}-\frac{6\gamma^2 X_0'Z_0'^2}{a^2D^2}-pZ_0'+\frac{3\gamma q Z_0'^2}{aD}\right.$$
$$\left.-\frac{3\gamma X_0'}{aD}(qX_0'-pY_0')-\frac{6\gamma^2 X_0 Z_0'^2}{a^2D^3}\right]$$

$$Y_{ao}''' = -a^2\gamma\left[Y_0'+\frac{3\gamma X_0'Z_0'}{aD}-\frac{6\gamma^2 Y_0'Z_0'^2}{a^2D^2}-qZ_0'-\frac{3\gamma p Z_0'^2}{aD}\right.$$
$$\left.-\frac{3\gamma Y_0'}{aD}(qX_0'-pY_0')-\frac{6\gamma^2 Y_0 Z_0'^2}{a^2D^3}\right]$$

$$X_{ao}^{(iv)} = -a^3\gamma\left[Y_0'+4\frac{\gamma X_0'Z_0'}{aD}-12\frac{\gamma^2 Y_0'Z_0'^2}{a^2D^2}\right]$$

$$Y_{ao}^{(iv)} = a^3\gamma\left[X_0'-4\frac{\gamma Y_0'Z_0'}{aD}-12\frac{\gamma^2 X_0'Z_0'^2}{a^2D^2}\right]$$

The terms X_{ao}''' and Y_{ao}''' are evaluated including only terms of first order in $p, q, \frac{X_0}{D}, \frac{Y_0}{D}, \frac{Z_0}{D}$. The terms $X_{ao}^{(iv)}$ and $Y_{ao}^{(iv)}$ are evaluated including only zero order terms.

The parameter s_a is now defined by the following relation:

$$\left(\frac{ds_a}{ds}\right)^2 = \left(\frac{dX_a}{ds}\right)^2 + \left(\frac{dY_a}{ds}\right)^2$$

$$= K^2(1+a_1 s+\tfrac{1}{2}a_2 s^2+\tfrac{1}{6}a_3 s^3+\ldots)$$

where

$$K^2 = X_{ao}'^2+Y_{ao}'^2$$

$$a_1 = \tfrac{2}{K^2}(X_{ao}''X_{ao}'+Y_{ao}''Y_{ao}')$$

$$a_2 = \tfrac{2}{K^2}(X_{ao}''^2+Y_{ao}''^2+X_{ao}'''X_{ao}'+Y_{ao}'''Y_{ao}')$$

$$a_3 = \tfrac{4}{K^2}(X_{ao}^{(iv)}X_{ao}'+Y_{ao}^{(iv)}Y_{ao}') + \tfrac{6}{K^2}(X_{ao}'''X_{ao}''+Y_{ao}'''Y_{ao}'')$$

Extracting the square root and integrating:

$$\frac{s_a}{s} = K[1+\tfrac{1}{4}a_1 s +\tfrac{1}{12}(a_2-\tfrac{1}{2}a_1^2)s^2+\tfrac{1}{18}(\tfrac{1}{8}a_3-\tfrac{1}{2}a_1a_2)s^3+\ldots$$

We must solve this equation for s in terms of s_a:

$$s = \frac{s_a}{K}[1+b_1 s_a +\tfrac{1}{2}b_2 s_a^2+\tfrac{1}{6}b_3 s_a^3+\ldots]$$

We shall see that it is only necessary to solve for b_1 and b_2.

$$b_1 = -\frac{a_1}{4K} \qquad\qquad b_2 = \frac{1}{3K}(a_1^2-\tfrac{1}{2}a_2)$$

The substitution for s in the equations we have derived enables us to express them in terms of the parameter s_a:

$$X_a = X_{bo}+X_{bo}'s_a+\tfrac{1}{2}X_{bo}''s_a^2+\tfrac{1}{6}X_{bo}'''s_a^3+\tfrac{1}{24}X_{bo}^{(iv)}s_a^4$$

$$Y_a = Y_{bo}+Y_{bo}'s_a+\tfrac{1}{2}Y_{bo}''s_a^2+\tfrac{1}{6}Y_{bo}'''s_a^3+\tfrac{1}{24}Y_{bo}^{(iv)}s_a^4$$

where $X_{bo} = X_{ao}$ $\qquad\qquad X_{bo}' = \frac{1}{K}X_{ao}'$

$$X_{bo}'' = \frac{1}{K^2}(X_{ao}''+2Kb_1X_{ao}')$$

$$X_{bo}''' = \frac{1}{K^3}(X_{ao}'''+6Kb_1X_{ao}''+3K^2b_2X_{ao}')$$

$$X_{bo}^{(iv)} = \frac{1}{K^4}[X_{ao}^{(iv)}+12Kb_1X_{ao}'''+12K^2(b_1^2+b_2)X_{ao}''+4K^3b_3X_{ao}']$$

There are similar expressions for $Y_{bo}^{(i)}$.

D. Calculation of the Sagitta of the Projected Track

At this point we wish to calculate a quantity which characterizes the curvature. The quantity we shall use is the sagitta of the projected track at its center point. Let us measure s_a from the center point of the projected track. Then the perpendicular distance from a point on the track to the line tangent at $s_a = 0$ is given by

$$\delta = \delta_1 + \delta_2 + \delta_3$$

where

$$\delta_1 = \tfrac{1}{2} s_a{}^2 (X_{bo}''Y_{bo}' - Y_{bo}''X_{bo}')$$

$$\delta_2 = \tfrac{1}{6} s_a{}^3 (X_{bo}'''Y_{bo}' - Y_{bo}'''X_{bo}')$$

$$\delta_3 = \tfrac{1}{24} s_a{}^4 (X_{bo}^{(iv)} Y_{bo}' - Y_{bo}^{(iv)} X_{bo}')$$

It is convenient to define quantities which represent the values that the δ's would have if the relation between s and s_a were linear:

$$\delta_{10} = \frac{s_a{}^2}{2K^3} (X_{ao}''Y_{ao}' - Y_{ao}''X_{ao}')$$

$$\delta_{20} = \frac{s_a{}^3}{6K^4} (X_{ao}'''Y_{ao}' - Y_{ao}'''X_{ao}')$$

$$\delta_{30} = \frac{s_a{}^4}{24K^5} (X_{ao}^{(iv)} Y_{ao}' - Y_{ao}^{(iv)} X_{ao}')$$

In terms of these quantities,

$$\delta_1 = \delta_{10}$$

$$\delta_2 = \delta_{20} + 2b_1 s_a \delta_{10}$$

$$\delta_3 = \delta_{30} + 3b_1 s_a \delta_{20} + (b_1{}^2 + b_2) s_a{}^2 \delta_{10}$$

We notice that b_3 does not enter into these equations. Also b_1 and b_2 enter only into the δ_2 and δ_3 correction terms, thus we only need to evaluate them approximately.

We can see from the figure that

$$\delta_a \approx \frac{\delta_1 + \delta_3}{\cos \varphi}$$

where $\quad \varphi \approx \tan^{-1} \dfrac{\delta_2}{s_a}$
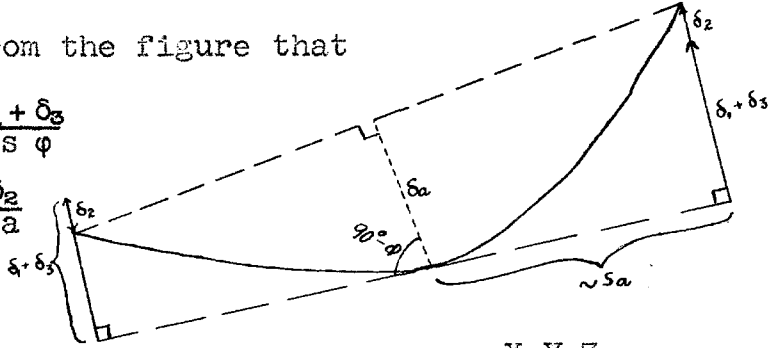
In actual measurements $p, q \ll 1$ and also $\dfrac{X}{D}, \dfrac{Y}{D}, \dfrac{Z}{D} \ll 1$. Thus we shall neglect high powers of these quantities in the δ_2 and δ_3 correction terms.

In order to organize our computations, we shall define the following quantities:

$$A = \frac{\gamma Z_0'}{(1 - Z_0'^2)} \left\{ \frac{X_0}{D} X_0' + \frac{Y_0}{D} Y_0' \right\}$$

$$B = \frac{Z_0'}{(1 - Z_0'^2)} (p X_0' + q Y_0')$$

$$C = \frac{\gamma^2 Z_0'^2}{(1 - Z_0'^2)} \left\{ \left(\frac{X_0}{D} \right)^2 + \left(\frac{Y_0}{D} \right)^2 \right\}$$

$$D' = \frac{\gamma (q X_0' - p Y_0')}{(1 - Z_0'^2)} \left\{ \frac{Y_0}{D} X_0' - \frac{X_0}{D} Y_0' \right\}$$

$$E = \frac{\gamma Z_0'^2}{(1 - Z_0'^2)} \left\{ p \frac{X_0}{D} + q \frac{Y_0}{D} \right\}$$

In terms of these quantities,

$$K^2 = \gamma^2 (1 - Z_0'^2)(1 + 2A + C)$$

$$\delta_1 = \delta_{1a} = \frac{e B_z s_a^2 (1 + A - B - D' - E)}{2 P \gamma \{(1 - Z_0'^2)(1 + 2A + C)^3\}^{\frac{1}{2}}}$$

This latter equation can now be solved for the one unknown quantity P.

The correction terms, δ_2 and δ_3, depend on higher powers of $a = \dfrac{e B_z}{P}$. However, we can substitute into them an approximate value of a given by neglecting all correc-

tion terms and approximating the track by a circle of radius
$\rho_a = \frac{s_a^2}{2\delta_a}$.

The next step will be to evaluate these correction terms. As we have seen δ_3 is added to δ_1 in the measured sagitta whereas δ_2 only serves to rotate the chord by an angle φ. The correction factor $\cos\varphi$ is negligible and will be ignored. However, δ_2 will serve to distort the projection from a symmetrical form, and thus a direct comparison of the photograph of the track with a circular arc is likely to give a misleading result. It should be emphasized that the pertinent quantity for the present calculation is the apparent sagitta.

We shall now evaluate the a's and b's, in the process neglecting high powers of $p, q, \frac{X}{D}, \frac{Y}{D}, \frac{Z}{D}$.

$$a_1 = \frac{4\gamma Z_0'}{D} - 2aZ_0'(F+G)$$

$$a_2 = \frac{20\gamma^2 Z_0'^2}{D^2}$$

where we have defined $F = \frac{qX_0' - pY_0'}{1 - Z_0'^2}$

$$G = \frac{\gamma}{(1 - Z_0'^2)}\left\{\frac{Y_0}{D}X_0' - \frac{X_0}{D}Y_0'\right\}$$

Considering s_a to be measured to the ends of the track from the apparent center we get,

$$b_1 s_a = -\frac{\gamma \Delta Z}{2D} - \frac{\gamma^2(\Delta Z)^2}{4D^2} + \frac{a\Delta Z}{4}(F+G)$$

$$b_2 s_a^2 = \frac{\gamma^2(\Delta Z)^2}{2D^2} - \frac{4a\gamma(\Delta Z)^2}{3D}(F+G) + \frac{1}{8}a^2(\Delta Z)^2(F+G)^2$$

The approximate values for the sagittas which neglect

variations in magnification along the track become:

$$\delta_{20} = \delta_{10}\left\{\frac{\gamma\Delta Z}{2D}(1-A+\frac{\gamma\Delta Z}{2D})-\frac{a\Delta Z}{2}(F+G)\right\}$$

$$\delta_{30} = \delta_{10}\left\{\frac{\gamma^2(\Delta Z)^2}{4D^2}-\frac{1}{48}a^2L^2\right\}$$

where L is the true length of the chord of the track in
space and ΔZ is the change in Z co-ordinate between its
ends. Using the previously expressed relations we find,

$$\delta_2 = -\delta_{10}\left\{\frac{\gamma\Delta Z}{2D}(1+A-\frac{\gamma\Delta Z}{2D})-\frac{1}{5}a\Delta Z(F+G)\right\}$$

$$\delta_3 = \delta_{10}\left\{\frac{\gamma^2(\Delta Z)^2}{4D^2}-\frac{1}{48}a^2L^2-\frac{23a\gamma(\Delta Z)^2}{24D}(F+G)+\frac{13}{48}a^2(\Delta Z)^2(F+G)\right\}$$

We notice that the contribution to δ_2 and δ_3 from the
variation in the magnification is of the same order as
that from the nonlinearity of the conical projection.
In other words, δ_{20} and δ_2 are of the same order of
magnitude, but the coefficients have been changed appre-
ciably.

In making measurements on the projection it is con-
venient to measure L_a, the length of the chord, rather
than s_a, the half length of the arc. In applying a
correction factor it is sufficiently accurate to assume
the curve to be a circular arc of radius ρ_a. In this case

$$s_a^2 \approx \frac{L_a^2}{4}(1+\frac{L_a^2}{12\rho_a^2})$$

It is also convenient to factor out some of the terms
into one experimentally measured factor L/L_a, where L is
the true chord length in space. For the case of a straight

line $(a=0)$

$$\frac{s}{s_a} = \frac{1 + b_1 s_a + \frac{1}{2} b_2 s_a^2}{\gamma \sqrt{(1 - Z_0'^2)(1 + 2A + C)}}$$

where, when $a=0$, $b_1 s_a = -\dfrac{\gamma \Delta Z}{2D}$

$$b_2 s_a^2 = \frac{\gamma^2 (\Delta Z)^2}{2D^2}$$

Remembering that s_a is measured from the center of the projected track,

$$\frac{L}{L_a} = \frac{1 + \dfrac{\gamma^2 (\Delta Z)^2}{4D^2}}{\gamma \sqrt{(1 - Z_0'^2)(1 + 2A + C)}}$$

In many cloud chambers used for accurate momentum measurements the rear wall serves as the movable chamber piston. Thus the photograph, as well as its reprojection, is actually the projection of the track on the piston in its expanded position, whereas we should insert into our formula quantities measured when the chamber is compressed. The correction is very small so that the only appreciable effect is to divide all quantities measured directly on the conical projection by $(1 + \dfrac{\varepsilon Z_0}{DZ_0})$, where $(1 + \varepsilon)$ is the expansion ratio. However, since our formula will have an equal number of directly measured quantities in numerator and denominator this correction cancels out.

The final result of these calculations is the following formula:

$$P = eB_z \rho_a \frac{L}{L_a} (\Sigma)(1 + f)$$

where: $\rho_a = \dfrac{L_a^2}{8\delta_a}$

$$\Sigma = \frac{1+A-B-D'-E}{1+2A+C} \approx 1-A-B$$

$$f = \frac{3L_a^2}{48\rho_a^2} - \frac{23\gamma Z_0'\Delta Z L_a}{24D\rho_a}(F+G) + \frac{13Z_0'^2 L_a^2}{48\rho_a^2}(F+G)^2$$

This latter term incorporates the correction due to δ_3, the correction term in L/L_a, and the conversion from s_a to L_a. The A term is the first order correction for the effect of the conical projection. The B term is the first order correction for the X and Y components of the magnetic induction.

For $Z_0' < 0.4$ we make an error of less than 1% by neglecting C and E. D' is appreciable only in extreme cases of a track near the front edge of the chamber where $\dfrac{X}{D}, \dfrac{Y}{D}$ and also p, q become large.

E. Measurement of the Direction of the Track

Since it is difficult to construct accurately a tangent at the center of the projected track, it is convenient to assume that the direction cosines of the chord are a good approximation to the values of X_0', Y_0', Z_0'. To check that this procedure introduces only negligible errors we evaluate approximately the $\Delta X, \Delta Y, \Delta Z$ of the chord. If s_1 and s_2 are the values of s corresponding to the two ends of the track, then

$$\Delta X = X_0'(s_2-s_1) + \tfrac{1}{2}a Y_0'(s_2^2-s_1^2)$$

$$\Delta Y = Y_0'(s_2-s_1) - \tfrac{1}{2}a X_0'(s_2^2-s_1^2)$$

$$\Delta Z = Z_O'(s_2 - s_1) + \tfrac{1}{2}a(qX_O' - pY_O')(s_2^2 - s_1^2)$$

But $\quad s_2 - s_1 \approx L$

and $\quad s_2^2 - s_1^2 \approx \dfrac{4b_1}{K^2} s_a^2 = - \dfrac{Y\Delta Z}{2D}L^2$

Thus, $\quad \dfrac{\Delta X}{L} = X_O' - \tfrac{1}{4}\dfrac{La}{\rho_a}Y_O'\dfrac{Y\Delta Z}{D}$

$\qquad \dfrac{\Delta Y}{L} = Y_O' + \tfrac{1}{4}\dfrac{La}{\rho_a}X_O'\dfrac{Y\Delta Z}{D}$

$\qquad \dfrac{\Delta Z}{L} = Z_O' - \tfrac{1}{4}\dfrac{La}{\rho_a}(qX_O' - pY_O')\dfrac{Y\Delta Z}{D}$

Remembering that X_O' and Y_O' enter into the correction

terms only when multiplied by first order terms like $\dfrac{X_O}{D}$,

p, etc., the error made by replacing them by $\dfrac{\Delta X}{L}$ and $\dfrac{\Delta Y}{L}$

is always negligible. The correction to $\dfrac{\Delta Z}{L}$ is already

of the second order and thus has even smaller effect.

F. Effect of an Inhomogeneous Magnetic Field

In order to analyze the effect of a magnetic field

that varies over the length of the track, it is not con-

venient to use the rigorous solution to the equations of

motion. However, since we are interested only in a

correction term, the following less exact procedure is

justified.

Consider that for the purpose of evaluating the mag-

netic force, the velocity vector is fixed, having direction

cosines (X_O', Y_O', Z_O'). We can then determine the deflec-

tion of the track from the tangent line by evaluating the

integral:

$$\vec{\delta} = \frac{e}{P} \int_0^{\frac{L}{2}} \int_0^{\ell} (\frac{\vec{v}}{v} \times \vec{B})\, ds\, d\ell \approx \frac{e\vec{v}}{Pv} \times \int_0^{\frac{L}{2}} \int_0^{\ell} \vec{B}\, ds\, d\ell$$

To be more exact, the above integral should be carried out from the center to each end of the track, and the results averaged, to give a value for the true sagitta in space, which can then be projected onto the rear wall of the chamber. Thus we should insert into our previously derived equations an average value of B obtained from:

$$\overline{\vec{B}} = \frac{4}{L^2} \int_0^{\frac{L}{2}} \int_0^{\ell} \vec{B}\, ds\, d\ell + \frac{4}{L^2} \int_0^{\frac{-L}{2}} \int_0^{-\ell} \vec{B}\, ds\, d\ell$$

If we assume B_z, p, and q to vary linearly over the half lengths of the track, the values of $\vec{B}$ at points one-third of the distance from the center to the ends should be determined and then averaged. The result will be a good approximation to $\overline{\vec{B}}$. It should be noted that in a cloud chamber magnet the hole through the front pole piece for viewing the chamber decreases the field at its center. Thus, if a single track traverses a chamber from a high magnetic field at the top edge to a minimum at the center and back to a high value at the bottom, the above two linear approximations will be quite satisfactory; whereas, the magnetic field at the center of the track will be quite inappropriate as an average value.

G. Construction of the Tangent At One End of the Track

Consider a track whose conical projection is described by the equations:

$$X_a = X_{bo} + X_{bo}' s_a + \tfrac{1}{2} X_{bo}'' s_a^2 + \tfrac{1}{6} X_{bo}''' s_a^3 + \ldots$$

$$Y_a = Y_{bo} + Y_{bo}' s_a + \tfrac{1}{2} Y_{bo}'' s_a^2 + \tfrac{1}{6} Y_{bo}''' s_a^3 + \ldots$$

If s_a is measured from the center of the apparent view, the ends will be represented by $s_a = \pm s_{a1}$. We define the notation $[i,j] = X_{bo}^{(i)} X_{bo}^{(j)} + Y_{bo}^{(i)} Y_{bo}^{(j)}$. Then the length of the chord will be given by

$$L_a = 2 s_{a1} \{ 1 + \tfrac{1}{6} [1,3] s_{a1}^2 + 0^4 (\tfrac{s_{a1}}{\rho_a}) \}$$

We construct a point on the line tangent at $s_a = -s_{a1}$, at a distance L_a from this end.

$$X_{a_T} = X_{bo} - X_{bo}'(s_{a1} - L_a) + \tfrac{1}{2} X_{bo}''(s_{a1} - 2L_a)s_{a1} - \tfrac{1}{6} X_{bo}'''(s_{a1} - 3L_a)s_{a1}^2 + \ldots$$

$$Y_{a_T} = Y_{bo} - Y_{bo}'(s_{a1} - L_a) + \tfrac{1}{2} Y_{bo}''(s_{a1} - 2L_a)s_{a1} - \tfrac{1}{6} Y_{bo}'''(s_{a1} - 3L_a)s_{a1}^2 + \ldots$$

The distance from this point to the end of the chord is given by

$$\Delta X_{a_T} = X_{bo}'(L_a - 2s_{a1}) - X_{bo}'' s_{a1} L_a + \tfrac{1}{2} X_{bo}''' s_{a1}^2 (L_a - \tfrac{2}{3} s_{a1}) + \ldots$$

$$\Delta Y_{a_T} = Y_{bo}'(L_a - 2s_{a1}) - Y_{bo}'' s_{a1} L_a + \tfrac{1}{2} Y_{bo}''' s_{a1}^2 (L_a - \tfrac{2}{3} s_{a1}) + \ldots$$

$$\Delta_a = \sqrt{(\Delta X_{a_T})^2 + (\Delta Y_{a_T})^2}$$

$$= \tfrac{1}{2} L_a^2 [2,2]^{\frac{1}{2}} \left\{ 1 - \frac{L_a}{12[2,2]} \left(2[2,3] + [1,2][1,3] + 0^2 (\frac{L_a}{\rho_a}) \right) \right\}$$

Using the expressions derived in the momentum calculation it is possible to derive

to first order in $(\frac{Z_o' X}{D})$, $(\frac{Z_o' Y}{D})$, $(Z_o' p)$, or $(Z_o' q)$:

$$[2,2] = \frac{\alpha^2 (1 - 2B)}{\gamma^2 (1 - Z_o'^2)(1 + 2A)^2}$$

to zero order: $[2,3] = \dfrac{-3a^2 Z_0'^2}{D\gamma^2(1-Z_0'^2)^{3/2}}$

exactly: $[1,2] = 0$

(This equation re-emphasizes the fact that the acceleration is perpendicular to the velocity).

Combining these results we find

$$\Delta_a = \frac{La^2}{2\rho_a^2}\left(1+\frac{\gamma\Delta Z}{2D}\right)$$

The method used in applying this quantity to the construction of the tangents is demonstrated in Fig. 3 (page 11).

Another correction that must be applied in some extreme cases is due to the fact that nonaxial components of the magnetic field induce changes in Z' along the track. Thus the Z co-ordinate of the end of the tangent is slightly different from that of the end of the chord. The change can be seen directly from the expansion,

$$Z = Z_0 + Z_0's + \tfrac{1}{2}a(qX_0'-pY_0')s^2+\ldots$$

If we make the approximation that s is measured from the center of the track we find that

$$\Delta_Z = Z_T - Z_C = -\frac{La}{2\rho_a}L(qX_0'-pY_0')$$

III. DECAY DYNAMICS

A. Introduction

The purpose of this section is to analyze various modes of decay which might be applicable to neutral V-particles. The dynamics of two-body decays are the simplest, and most of the results listed herein have been used by investigators in analyzing their data.[1-4] The reasons for including the two-body decay dynamics here are two-fold: firstly, it is convenient to have the results in a single unified presentation; secondly, the two-body decay considerations form a useful introduction to the analysis of the more complicated three-body dynamics which follows.

It is important to analyze closely the dynamics of a two-body decay for two reasons. Firstly, many of the cloud chamber observations are far from ideal and the information gathered from such data may only be statistical in nature. It may be possible to set limits on the Q-value and other calculated quantities from limited information on a particular case. It is necessary to maximize information from even the poorest cases, because they have to be included in any statistical analysis, e. g. a calculation of the mean lifetime. Secondly, it is important to check on any bias which might be introduced by the chamber geometry and the selection of cases. A convenient technique to perform such checks is to repre-

sent the data on one of the plots described in the analysis of the two-body decay dynamics.

The decay of charged particles will not be discussed. However, a similar analysis can be carried out for charged V-particles and the results are analogous to those derived here.

The emphasis in the analysis of three-body decay dynamics will be on the properties of the charged decay products. For the purpose of comparison with experimental results it is important to consider the manifestations of a three-body decay when the charged products are analyzed as if they originated in a two-body decay. For example, the measured energy release, Q, for a single two-body decay should be unique within experimental errors. Therefore, it is useful to analyze the significance of the distribution of calculated Q'-values if the observed products actually originate in a three-body decay.

B. Notation

In an ideal cloud chamber observation of the decay of a neutral V-particle the following quantities are measured:

P_+, $P-$: the magnitude of the momenta of the charged products

θ : the angle between the momentum vectors of the charged products

I_+, $I-$: the specific ionization of the charged products. (Due to the difficulty of estimation of the ionizations they are in general known only roughly).

If an interaction in the solid material near the cloud chamber projects charged particles into the chamber, and if the V-particle is assumed to originate in that interaction, the following additional quantities can be measured:

θ_+, $\theta -$: the angles between the momentum vectors of the charged products and the line of flight of the V^o.

From the above data the following quantities can be calculated directly:

M_+, $M-$: the rest masses of the charged products. (Due to the large errors in most estimates of ionizations, the calculated masses have large errors. The usual procedure is to identify the masses with those of known particles for the remaining calculations).

Q' : the energy release calculated, assuming no neutral secondaries were emitted, from P_+, P_- and θ.

δ : the angle between the plane of the charged decay products and the line of flight of the V^o

$P_{T+} = P_+ \sin \theta_+$: the transverse momentum of the positive secondary

$P_{T-} = P_- \sin \theta_-$: the transverse momentum of the negative secondary

$P_T = \dfrac{P_+ P - \sin \theta}{\sqrt{P_+^2 + P-^2 + 2 P_+ P - \cos \theta}}$: the transverse momentum if a two-body decay is assumed.

$\Delta P_\perp$: the total unbalanced momentum of the charged products perpendicular to the line of flight of the V^o

$\Delta P_T = P_{T+} - P_{T-}$: this quantity is approximately the component of the unbalanced transverse momentum in the plane of the secondaries

$$a = \frac{P_+\cos\theta_+ - P_-\cos\theta_-}{P_+\cos\theta_+ + P_-\cos\theta_-}$$

: the distribution of this quantity gives an indication of the relative masses of the charged decay products

$$a' = \frac{P_+^2 - P_-^2}{P_+^2 + P_-^2 + 2P_+P_-\cos\theta}$$

: for a two-body decay this quantity is equal to a, but it can be calculated independently of the location of a possible origin for the V-particle

$$a'' = \frac{\sin(\theta_- - \theta_+)}{\sin\theta}$$

: for a two-body decay this is also equal to a, but it can be calculated independently of the momenta of the secondaries

In the following analysis quantities referred to the co-ordinate system in which the V^o-particle is at rest shall be denoted by primes. The direction of flight of the V^o shall be the X direction. All momenta, masses, and energies shall be given in energy units, so that the velocity of light is considered as unity. Momenta shall be designated by P, total energies by W, and kinetic energies by T.

C. Two-Body Decay Dynamics
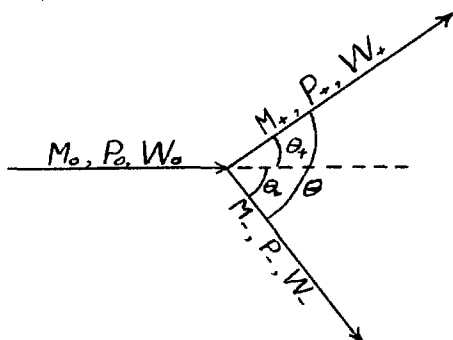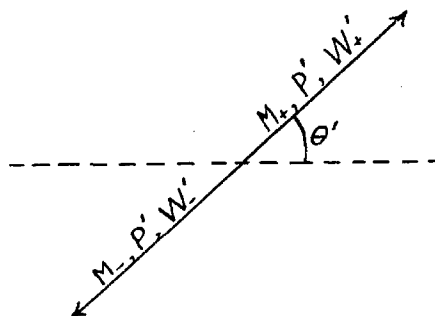
Laboratory System   Center of Mass System

Let us consider the two-body decay: $M_O \rightarrow M_+ + M_- + Q$. The pertinent quantities are defined in the figure above. Conservation of energy and momentum imply the following relations:

$$W_O = W_+ + W_-$$

$$P_O{}^2 = P_+{}^2 + P_-{}^2 + 2P_+P_-\cos\theta$$

$$P_+\sin\theta_+ = P_-\sin\theta_-$$

$$P' = \sqrt{Q^2\left(1-\frac{Q}{2M_O}\right)^2 + Q\left(1-\frac{Q}{2M_O}\right)\frac{2M_+M_-}{M_O}}$$

$$W_+{}' = M_+ + Q\left(1-\frac{M_+}{M_O} - \frac{Q}{2M_O}\right) \quad ; \quad W_-{}' = M_- + Q\left(1-\frac{M_-}{M_O} - \frac{Q}{2M_O}\right)$$

In a cloud chamber observation of a neutral V-particle decay, the most accurately measurable quantities are usually P_+, P_-, and θ. If we assume the masses of the secondary particles, the Q-value can be calculated,

$$Q = (M_+ + M_-)\left[\sqrt{1+\frac{2Q_1}{M_++M_-}} \quad -1\right]$$

where $Q_1 = \frac{1}{M_++M_-}[W_+W_- - M_+M_- - P_+P_-\cos\theta]$

If $Q_1 \ll M_+ + M_-$ the following expansion can be used conveniently:

$$Q = Q_1 - \frac{Q_1{}^2}{2(M_++M_-)} + \frac{Q_1{}^3}{2(M_++M_-)^2} - \cdots$$

It is convenient to calculate approximately the effect of errors in the momenta, angles and masses on the Q-value by using the relationships:

$$\frac{\partial Q}{\partial P_+} = \frac{1}{M_O}\left(\frac{W_-}{W_+}P_+ - P_-\cos\theta\right) \quad ; \quad \frac{\partial Q}{\partial P_-} = \frac{1}{M_O}\left(\frac{W_+}{W_-}P_- - P_+\cos\theta\right)$$

$$\frac{\partial Q}{\partial \theta} = \frac{P_+ P_- \sin\theta}{57.3 M_o} \text{ Mev/deg.}$$

$$\frac{\partial Q}{\partial M_+} = \frac{M_+}{M_o}(1 + \frac{W_-}{W_+}) - 1 \quad ; \quad \frac{\partial Q}{\partial M_-} = \frac{M_-}{M_o}(1 + \frac{W_+}{W_-}) - 1$$

Many photographs of V-particle disintegrations cannot yield accurate values for all the quantities we have assumed. Furthermore, it is inconvenient to carry out a complete computation of all these quantities for the relatively poor cases. In particular, it is more convenient to represent the data in a fashion which demonstrates their compatibility or incompatibility with certain assumed decay schemes and which checks the effects of observational bias on the isotropy of emission in the center of mass system. For this purpose it is convenient to make use of the following quantities:

$$a = \frac{P_+ \cos\theta_+ - P_- \cos\theta_-}{P_+ \cos\theta_+ + P_- \cos\theta_-} \quad ; \quad a_o = \frac{M_+^2 - M_-^2}{M_o^2}$$

$$a' = \frac{P_+^2 - P_-^2}{P_+^2 + P_-^2 + 2P_+ P_- \cos\theta} \quad ; \quad a'' = \frac{\sin(\theta_- - \theta_+)}{\sin\theta}$$

$$P_{T+} = P_+ \sin\theta_+ \quad ; \quad P_{T-} = P_- \sin\theta_-$$

$$P_T = \frac{P_+ P_- \sin\theta}{\sqrt{P_+^2 + P_-^2 + 2P_+ P_- \cos\theta}}$$

For an ideal two-body decay observation $a = a' = a''$ and $P_{T+} = P_{T-} = P_T$. The values may differ due to errors in measurement or due to a wrong identification of the origin of the V-particle. It should be noted that a' and P_T can be determined by measurements on the secondaries only.

In terms of the parameters which specify the decay

in the center of mass system,

$$P_T = P' \sin \theta'$$

$$\alpha = \alpha' = \alpha'' = \alpha_0 + \frac{2P' \cos \theta'}{M_0 \beta_0}$$

where $\beta_0 c$ is the velocity of the V^0. If the secondaries
are emitted isotropically in the center of mass system,
these quantities should have the following distributions:

$$\text{Prob}(P_T)dP_T = \frac{P_T \, dP_T}{P'(P'^2 - P_T^2)^{\frac{1}{2}}}$$

$$\text{Prob}(\alpha)d\alpha = \frac{M_0}{4P'}d\alpha \int_0 \beta_0 \text{Prob}(\beta_0)d\beta_0 \quad \begin{cases} 1; & \text{for } |\alpha - \alpha_0| \leqslant \frac{2P'}{M_0} \\ \frac{2P'}{M_0|\alpha-\alpha_0|} & \text{for } |\alpha-\alpha_0| \geqslant \frac{2P'}{M_0} \end{cases}$$

The distribution of P_T is sharply peaked at P'. Its
average is $\frac{\pi}{4}P'$ and its standard deviation is $.22P'$. The
peaked nature is due to the large solid angle per unit
angle near 90°. Experimental errors will make the peak
smoother but should not affect the average value appre-
ciably.

The distribution of α is symmetric about α_0. This
value gives us an estimate of the relative magnitude of
the secondary masses by using the inequality:

$$\frac{M_+}{M_-} \geqslant \frac{1+\alpha_0\left(1+\frac{2\delta}{M_0}\right)}{1-\alpha_0\left(1+\frac{2\delta}{M_0}\right)} > \frac{1+\alpha_0}{1-\alpha_0} \qquad (M_+ \geqslant M_-)$$

The central region of the distribution $(|\alpha - \alpha_0| \leqslant \frac{2P'}{M_0})$ is
flat and has a height $\frac{M_0}{4P'}\beta_{0\,av}$. For a distribution of β_0
which is peaked near $\beta_0 = 1$, the standard deviation of the
distribution of α is of the order of the width of this flat
region. For example, if we assume $\text{Prob}(\beta_0)d\beta_0 = 3\beta_0^2 d\beta_0$,

then $\sigma(\alpha) = \frac{2P'}{M_O}$. In actual cloud chamber observations such a distribution would not be surprising since the very slow V^O's decay before reaching the illuminated volume, and many fast cases are observed. It is important that no bias toward certain angles in the center of mass system be introduced by the selection of cases. For example, the requirement that both momenta be well measurable tends to favor cases in which the heavier secondary is emitted backwards because it receives a larger fraction of the primary momentum than the lighter secondary.

A number of plots have been found useful for representing V-particle data and checking their consistency with various decay modes. One of the most important has been the "Q-plot":[3,4] a plot of P_T vs. α (Fig. 4). In terms of the constants of the decay the theoretical relation between P_T and α for a given primary momentum is represented by

$$(\alpha-\alpha_O)^2 + (\frac{2P_T}{M_O\beta_O})^2 = (\frac{2P'}{M_O\beta_O})^2$$

Thus the curves of P_T vs. α for constant P_O are ellipses, centered about $\alpha = \alpha_O$, $P_T = 0$, which approach a limiting ellipse as $\beta_O \rightarrow 1$. This representation is very useful for cases in which the primary is of high momentum so that $\beta_O \approx 1$. In this case the secondaries are usually also very fast so that their ionization is almost minimum and they cannot be identified. However, by observing the
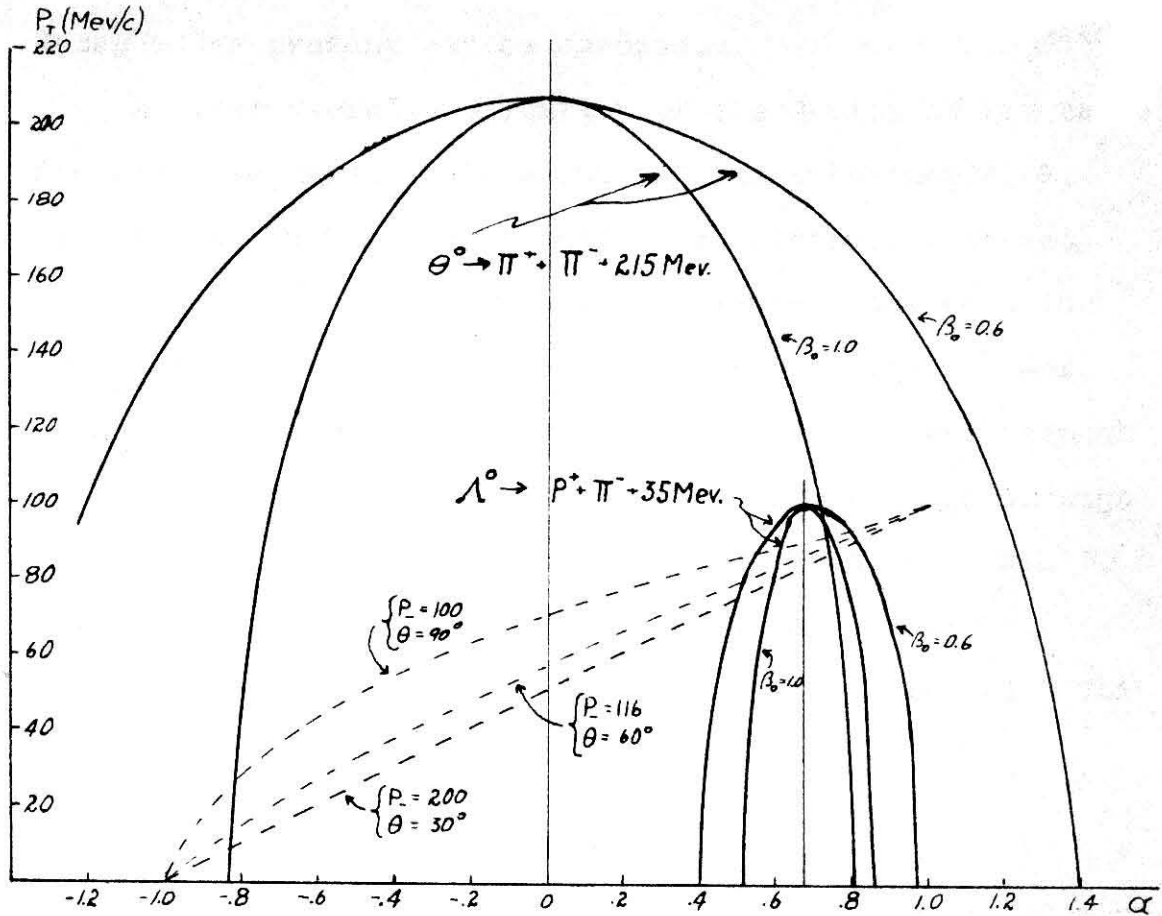
Fig. 4. Q-Plot

The dashed lines are curves of P_T vs. α as P_+ is allowed to vary, if P_- and θ are fixed. The three curves all correspond to $P_- \sin\theta = 100$ Mev/c. The curve for $\theta = 30°$ is almost a straight line, as are the curves for smaller angles. In general, the intercept on the P_T axis ($\alpha = 0$) is $P_- \sin\theta/2$.

distribution of points on the Q-plot, the nature of the decay modes present can be guessed.

Another useful application of the Q-plot is for cases in which the negative momentum and the total angle, θ, are accurately known, but only rough limits can be set on the positive momentum. If we calculate the behavior of P_T vs. α as P_+ varies we find that the curve passes through $(1, P_- \sin\theta)$ with slope $\frac{1}{2} P_- \sin\theta$ when $P_+ \to \infty$, through $(0, P_- \sin\theta/2)$ with slope $P_- \sin\theta/2$ when $P_+ = P_-$, and through $(-1, 0)$ with slope $\frac{1}{2} P_- \tan\theta$ when $P_+ = 0$. Thus for small θ, the curve of P_T vs. α as P_+ varies is approximately a straight line passing through $(1, P_- \sin\theta)$ and $(-1, 0)$. This fact can be seen from the exact relation[*]

$$\frac{2P_T}{1+\alpha} = P_- \sin\theta \sqrt{1 + \left(\frac{P_- \sin\theta}{P_+ + P_- \cos\theta}\right)^2}$$

This relation is also useful in assigning error vectors on the α vs. P_T plot. If θ is small, or $P_- \ll P_+$, the error vector due to an error in P_+ must point to $(-1, 0)$. If θ is small a similar argument predicts that the error vector due to an error in P_- must point to $(1, 0)$. Since α is dimensionless in the momenta it can be seen that an error in calibration of the magnetic field would produce an error vector parallel to the P_T axis because it would multiply all momenta by a constant factor.

---

[*]This relation was pointed out to the author by Dr. R. V. Adams.

As a check on the isotropy of emission in the center of mass system, one can use the relation $P_T = P'\sin\theta'$, to draw lines at equal intervals of $\cos\theta'$ on the Q-plot. If the emission is indeed isotropic, there should be equal numbers of points in each of the intervals on each branch of the ellipse. This procedure is equivalent to checking the distribution of P_T.

It should be noted, in applying the Q-plot to cases for which P_+ is uncertain, that each part of the P_+ error vector may correspond to a slightly different value of β_O. Thus in checking the consistency of a case with a particular decay scheme, the variation of β_O along the error vector must be included. However, for those cases in which P_+ is uncertain, β_O is usually very nearly unity so that the variation of β_O is small. This convenience does not apply to the other plots to be discussed here.

When dealing with data taken from a cloud chamber with no magnetic field, the momenta cannot be found directly. However, in a multiplate chamber the origin can often be located accurately. Thus the angles θ_+ and θ_- can be measured and α can be calculated. Another quantity which can be calculated from the angles is

$$\frac{2P_T}{P_O} = \frac{2\sin\theta_+\sin\theta_-}{\sin\theta}$$

Therefore, it is convenient to plot multiplate chamber data on a $\frac{2P_T}{P_O}$ vs. α plot. On such a plot the lines of

constant θ are universal circles, independent of the decay mode, given by the equation

$$a^2 + (\frac{2P_T}{P_O} + \cot\theta)^2 = \csc^2\theta$$

Thus a calculation of a or $\frac{2P_T}{P_O}$, together with the knowledge of the total angle, is sufficient to locate a point on the plot.

To check the consistency of events with a particular mode of decay, further information is needed. If one of the secondaries is stopped in one of the absorbing plates in the chamber by Coulomb interactions only, its residual range at the point of emission can be measured. In addition, if its mass can be inferred by combining its residual range with ionization estimates or scattering measurements, its initial momentum can be calculated, and therefore its momentum transverse to the line of flight of the V^O is known. The transverse momentum can then be compared with the value predicted by a particular decay scheme using the hyperbolas for constant P_T:

$$(a-a_O)^2 - (\frac{2P_T}{P_O})^2 (\frac{P'^2 - P_T^2}{P_T^2}) = \frac{4(P'^2 - P_T^2)}{M_O^2}$$

or the ellipses for constant P_O:

$$(a-a_O)^2 + (\frac{2P_T}{P_O})^2 (\frac{P_O^2 + M_O^2}{M_O^2}) = (\frac{2P'}{P_O})^2 (\frac{P_O^2 + M_O^2}{M_O^2})$$

Isotropy of emission in the center of mass can be checked using the hyperbolas of constant $\cos\theta'$:

$$(a-a_O)^2 - (\frac{2P_T}{P_O})^2 \cot^2\theta' = (\frac{2P'}{M_O})^2 \cos^2\theta'$$

It is also useful to study the behavior of the total
angle between the secondaries. It can be expressed in
terms of the primary momentum and the constants of the
decay:

$$\tan\theta = \frac{M_0{}^2 P_0 P' \sin\theta'}{(P_0 W_+{}' + W_0 P' \cos\theta')(P_0 W_-{}' - W_0 P' \cos\theta') - M_0{}^2 P'^2 \sin^2\theta'}$$

The behavior of this angle can be visualized best by
considering the following diagram representing the rela-
tivistic vector addition of momenta: $(M_+ \geqslant M_-)$
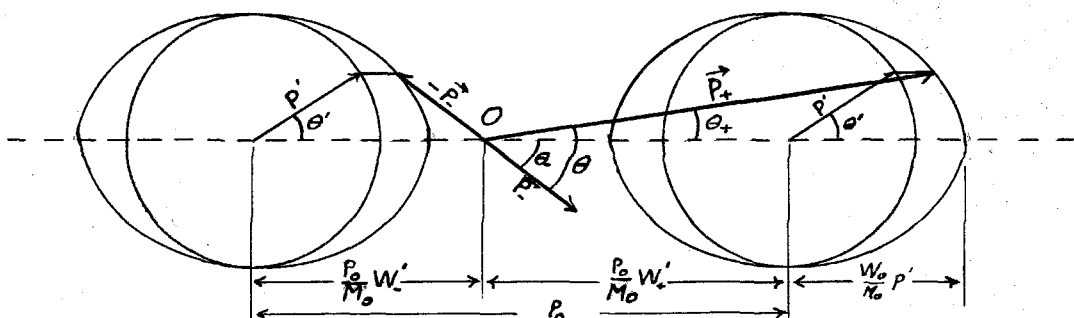
A study of the Lorentz transformation of momenta will
convince one that the vectors $\vec{P_+}$, and $\vec{P_-}$ are indeed the
laboratory momenta of the secondaries. At very low momen-
ta $(P_0 \leqslant M_0 \frac{P'}{M_+})$ the point O lies within both ellipses and
low angles are excluded. The minimum value of θ decreases
with increasing P_0 until just below the transition $P_0 = M_0 \frac{P'}{M_+}$,
the minimum value of θ is $\leqslant 90^O$. At a value of the momentum
larger than $M_0 \frac{P'}{M_+}$ but smaller than $M_0 \frac{P'}{M_-}$ all angles, θ, are
allowed. But at P_0 just larger than $M_0 \frac{P'}{M_-}$ angles above $\geqslant 90^O$
are forbidden. This upper limit on θ then decreases for
increasing momenta.

For many high energy V-particle decays, the total

angle can give a rough estimate of the primary momentum
if the nature of the decay is assumed. For high energy
V-particles the distribution of the angle, θ, is highly
peaked near the value corresponding to $\theta' = 90°$. Also
neglecting $M_O^2 P'^2$ compared to $P_O^2 W_+' W_-'$ we get the
estimate:

$$P_O \approx \frac{M_O^2 P'}{W_+' W_-' \theta}$$

This value will in general be close to a lower limit, but
will still be a good estimate of P_O.

D. Relation Between Two-Body and Three-Body Decays

If all or part of the observed V^O-particle decays
have three secondaries, one of which is neutral, calcula-
tions based on the assumption of a two-body decay will
give inconsistent results. However, it will still be
useful to calculate the Q'-value, based on the assumption
of two-body decay, and correlate the observed statistical
distribution of Q' with that expected from a three-body
decay. Likewise, it should be the aim of an analysis of
a three-body decay scheme to predict the distribution
of quantities which can be measured by making observations
on the charged secondaries and the origin of the V^O-
particle: e. g. $Q', a, \Delta P_T, \Delta P_\perp, \delta, P_T$.

Firstly we will derive the significance of the

distribution of Q'.[*] If M_O' is the "primary mass" calculated assuming a two-body decay, we see that the following equations serve to define the procedures for calculating M_O and M_O': (M_n is the mass of the neutral particle in this writing).

$$M_O{}^2 = (W_n + W_+ + W_-)^2 - (\vec{P_n} + \vec{P_+} + \vec{P_-})^2$$

$$M_O{}'^2 = (W_+ + W_-)^2 - (\vec{P_+} + \vec{P_-})^2$$

Thus it follows:

$$M_O{}'^2 = (M_O - M_n)^2 - 2(M_O T_n + M_n T_O) - 2T_O T_n + 2\vec{P_O} \cdot \vec{P_n}$$

Since we have made no assumptions concerning the Lorentz system in which the above equation has been derived; or, alternatively, since the basic equations are in a relativistically invariant form, we can evaluate the expressions in the center of mass system, ($T_O' = \vec{P_O}' = 0$).

Thus $M_O{}'^2 = (M_O - M_n)^2 - 2M_O T_n'$

or, in terms of the Q-value,

$$Q' = Q \frac{Q + 2(M_+ + M_-)}{Q' + 2(M_+ + M_-)} (1 - \frac{T_n'}{T_n'{}_{max}})$$

where $T_n'{}_{max} = Q(1 - \frac{M_n}{M_O} - \frac{Q}{2M_O})$

If $T_n'{}_{max} \ll M_O - M_n$

Then $Q' = Q - \frac{T_n'}{1 - \frac{M_n}{M_o}} - \frac{1}{2} \frac{T_n'^2}{M_O(1 - \frac{M_n}{M_o})^3} - \cdots$

or, in a different form, if $Q \ll M_+ + M_-$

Then $Q' = Q(1 - \frac{T_n'}{T_n'{}_{max}})(1 + \frac{Q T_n'}{2(M_+ + M_-)T_n'{}_{max}} + \cdots)$

---

[*]The following derivation and result was first pointed out by Dr. R. P. Feynman.

$T_n'max$ is the value of T_n' corresponding to M_+ and M_- being emitted in the center of mass system with the same velocity. In any case it is clear that the quantity which determines the "two-body energy release", Q', is the energy of the neutral particle in the center of mass system, and its distribution between 0 and Q is determined by the distribution of T_n'.

The total unbalanced momentum perpendicular to the line of flight of the V^0-particle is equal in magnitude to the component of P_n' perpendicular to the incident direction. If there is no coupling between the direction of motion of the V^0-particle and the decay in the center of mass system we can see that the distribution of $\Delta P_\perp$ should be:
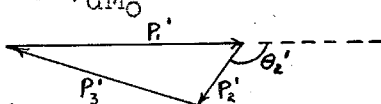
$$\text{Prob}(\Delta P_\perp)d(\Delta P_\perp) = \Delta P_\perp \int_{\Delta P_\perp}^{P_n'max} \frac{\text{Prob}(P_n')dP_n'}{P_n'\sqrt{P_n'^2 - \Delta P_\perp^2}}\, d(\Delta P_\perp)$$

The distributions of α and other quantities are much more difficult to evaluate. Only with specific assumptions regarding the decay scheme and the energies involved can we get an idea of their behavior. Therefore we will discuss them together with the specific assumed schemes.

E. General Three-Body Decay

We shall consider the general three-body decay in the center of mass system. Thus the constraints on the

system are that $\vec{P_1}' + \vec{P_2}' + \vec{P_3}' = 0; W_1' + W_2' + W_3' = M_0$. In

general we shall be interested in the distribution in

energy or momentum of the neutral secondary, which will

be chosen as M_1. As we have seen, the distribution of

T_1' determines the distribution of "two-body" Q'-values.

Since we shall assume no correlation between the direction

of motion of the primary particle and the decay in the

center of mass system, the distribution of P_1' will also

determine the distribution of unbalanced momentum. In

general,

$$\text{Prob}(P_1')dP_1'd\Omega_1' = \int_{\Omega_2'} f(P_1',P_2',\theta_2')\frac{dn}{dM_0}$$

where the density of states is given by

$$\frac{dn}{dM_0} = K\frac{P_1'^2 P_2'^2 dP_1' dP_2' d\Omega_1' d\Omega_2'}{dM_0}$$

$$= K\frac{P_1'^2 P_2'^3 W_2' W_3' d\Omega_1' d\Omega_2' dP_1'}{P_2'^2(M_0-W_1')+W_2'P_1'P_2'\cos\theta_2'}$$

where K is a normalization constant and $f(P_1',P_2',\theta_2')$ is

determined from the matrix element involved in the transi-

tion from the initial to the final state. An alternative

form of this formula is sometimes useful for computational

purposes:

$$\text{Prob}(P_1')dP_1' = KP_1'^2 dP_1'\frac{d}{dM_0}\int_{\Omega_2'}\int_{\Pi=0}^{P_2'(P_1',\theta_2',M_0,M_1)} f(P_1',\Pi',\theta_2')\Pi'^2 d\Pi' d\Omega_2'$$

This expression is particularly useful if we are going

to perform the integration over Ω_2', since the integrations

are usually much easier to perform before the differentia-

tion.

When the mass of one of the secondaries (for example M_3) is very large, so that its kinetic energy is negligible compared to T_1' and T_2', we can see, by analogy with beta decay theory, that $f(P_1', P_2', \theta_2')$ should include a factor $(P_1'^2 + 2P_1'P_2'\cos\theta_2' + P_2'^2)^\ell$, where the product particles are to carry away an orbital angular momentum of $\ell \hbar$. In this case the expression for $P_2'(P_1', \theta_2', M_0, M_1)$ is independent of θ_2'. Thus, if there are no further factors depending on θ_2' in f, the integration over Ω_2' can be performed first. Furthermore, if there are no other factors in f we can get an expression for the distribution of P_1':

$$\text{Prob}(P_1')dP_1' = 2KW_2' \sum_{s=0}^{\ell} \frac{(2\ell+1)!}{(2\ell-2s+1)!(2s+1)!} P_1'^{2s+2} P_2'^{2\ell-2s+1}$$

F. Uncoupled Three-Body Decay

If there is no coupling between the emitted particles $f(P_1', P_2', \theta_2') = 1$, we can proceed to evaluate the probability rigorously. We notice that the integral

$$I = \int_{\Omega_2'} \int \int^{P_2'} \Pi^2 d\Pi d\Omega_2'$$

is just the volume of the figure in a three-dimensional momentum space (ξ, η, ζ) whose bounding surface is the locus of possible values of the momentum vector $\vec{P_2'}$. The constraint is imposed by conservation of energy,
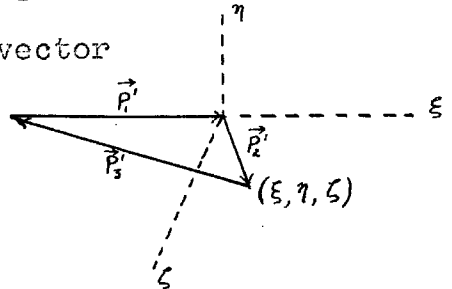
namely:

$$W_1' + \sqrt{\xi^2 + \eta^2 + \zeta^2 + M_2^2} + \sqrt{(\xi + P_1')^2 + \eta^2 + \zeta^2 + M_3^2} = M_0$$

This becomes the formula for a prolate spheroid:

$$\frac{(\xi - h)^2}{a^2} + \frac{\eta^2 + \zeta^2}{b^2} = 1$$

where $a^2 = \dfrac{W'^2 M_0^2}{(W'^2 - P_1'^2)^2} (W_{1m}' - W_1')(W_{1\mu}' - W_1')$

$b^2 = \dfrac{M_0^2}{(W'^2 - P_1'^2)} (W_{1m}' - W_1')(W_{1\mu}' - W_1')$

$h = \dfrac{P_1'}{2(W'^2 - P_1'^2)} (2M_0 W_1' - M_0^2 - M_1^2 - M_2^2 + M_3^2)$

where $W' = M_0 - W_1' = W_2' + W_3'$

$W_{1m}' = \dfrac{1}{2M_0}[M_0^2 + M_1^2 - (M_2 + M_3)^2] = M_1 + \dfrac{Q}{2M_0}(Q + 2M_2 + 2M_3)$

$W_{1\mu}' = \dfrac{1}{2M_0}[M_0^2 + M_1^2 - (M_2 - M_3)^2] = M_1 + \dfrac{1}{2M_0}(Q + 2M_2)(Q + 2M_3)$

W_{1m}' is the maximum total energy particle M_1 can have. Both a and b vanish, namely, the spheroid shrinks to a point, when W_1' attains this maximum value. The root $W_1' = W_{1\mu}'$ is unattainable and corresponds to one energy having a negative value; it is always larger than W_{1m}'.

Now we can evaluate I as the volume of this spheroid, namely $4/3\pi ab^2$.

$$I = \frac{4\pi}{3} \frac{M_0^3 (W_{1m}' - W_1')^{3/2} (W_{1\mu}' - W_1')^{3/2} (M_0 - W_1')}{(M_0^2 - 2M_0 W_1' + M_1^2)^2}$$

The only remaining step is the differentiation, which is cumbersome but straight-forward:

$$\text{Prob}(P_1')dP_1' = dP_1' \frac{2\pi K P_1'^2 (W_{1m}' - W_1')^{1/2} (W_{1\mu}' - W_1')^{1/2}}{3\left(1 - \frac{2W_1'}{M_0} + \frac{M_1^2}{M_0^2}\right)^3} U(W_1')$$

where, $U(W_1') = 3(1- \frac{W_1'}{M_O})^2 (1- \frac{2W_1'}{M_O} + \frac{M_1^2}{M_O^2})(W_{1m}'+W_{1\mu}'-2W_1')$

$\qquad - \frac{2}{M_O}(W_{1m}'-W_1')(W_{1\mu}'-W_1')(3- \frac{6W_1'}{M_O} + \frac{4W_1'^2}{M_O^2} - \frac{M_1^2}{M_O^2})$

It can be noted that it would be a very tedious task to arrive at such an expression from an integration over angles of $\frac{dn}{dM_O}$.

Some approximate expressions are especially useful. Firstly, if M_3 is very large so that $T_3' << Q$, we get the formula, (5)

$\qquad \text{Prob}(P_1')dP_1' = 4\pi K P_1'^2 P_2' W_2' dP_1'$

Secondly, if $W_{1m}' << M_O$,

$\qquad \text{Prob}(P_1')dP_1' = 2\pi K P_1'^2 (W_{1m}'-W_1') \; (W_{1\mu}'-W_1') \; x$
$\qquad\qquad\qquad\qquad\qquad\qquad\qquad (W_{1m}'+W_{1\mu}'-2W_1')$

We note that the expression for the probability distribution of P_1', when M_3 is very large, can be gotten easily by integrating the expression for $\frac{dn}{dM_O}$ in this approximation, since the latter is then independent of θ_2'. Furthermore, in this particular case we can insert any $f(\theta_2')$ without affecting the distribution of P_1'.

G. Cascade Three-Body Decay

Another type of decay scheme that should be considered is one in which the primary undergoes a two-body decay, but one of the secondaries undergoes another two-body decay so rapidly that only the two charged end products can be observed in the cloud chamber. Consider the decay

scheme: $M_O \rightarrow M_1 + M_* + Q_1$

$\quad\quad\quad\quad\quad \rightarrow M_2 + M_3 + Q_2$

Quantities in the system in which M_O is at rest (center
of mass system) will be denoted by primes, quantities in
the system in which M_* is at rest by double primes.

Two types of decays should be considered: those in
which M_1 and M_* are neutral particles (type I) and those
in which M_1 and M_* are charged particles and M_3 is a
neutral particle (type II). Decays of type I are simpler
and will be considered first.

In the center of mass system of cascade decays of
type I, the neutral product, M_1, has a unique energy W_1'
and a unique momentum P' determined by the conservation of
energy and momentum in the two-body decay $M_O \rightarrow M_1 + M_* + Q_1$.
Calculations from the measurements on the charged products
M_2 and M_3 will yield a unique value of Q', namely Q_2, and
the two-body distribution of P_T and α'. The only evidence
for such a decay scheme would come from the location of
the origin of the primary particle. The cascade decay
scheme would manifest itself by yielding a distribution
of $\Delta P_\perp$ determined by the momentum of the neutral secondary,
M_1.

$$\text{Prob}(\Delta P_\perp)\, d(\Delta P_\perp) = \frac{\Delta P_\perp \, d(\Delta P_\perp)}{P'\sqrt{P'^2 - (\Delta P_\perp)^2}}$$

If Q_1 were small compared to Q_2, such a decay scheme
would be very difficult to distinguish from a simple two-

body decay in which errors of measurement produced the observed distribution of ΔP_1.

Cascade decay II has more interesting manifestations. The distribution of the energy of the neutral secondary, M_3, in the center of mass system determines the distribution of the "two-body energy release", Q'. In terms of the parameters of the decay

$$W_3' = \frac{W_*'W_3'' + P'P''\cos\theta''}{M_*}$$

where W_*' and P' are the total energy and momentum of M_* in the center of mass system, and W_3'', P'', and θ'' are the energy, momentum and polar angle of emission of M_3 in the system in which M_* is at rest. If the second decay is isotropic in its center of mass system, $\cos\theta''$ is distributed uniformly between -1 and 1. Thus, the distribution of W_3' is uniform between the limits $\frac{1}{M_*}(W_*'W_3'' \pm P'P'')$. If $Q_1 + Q_2 << M_0 - M_3$ this distribution implies an almost uniform distribution of Q' centered about $Q_1 + Q_2 - \frac{1}{M_*}(W_*'W_3'' - M_*M_3)(\frac{M_0}{M_0-M_3})$

with a half width $\frac{P'P''M_0}{M_*(M_0-M_3)}$.

This distribution does not necessarily reach 0 or Q, as distinct from the general three-body decay. The reason lies in the fact that T_3' can be zero only if $\frac{P'}{M_*} = \frac{P''}{M_3}$; and that the condition when M_1 and M_2 are emitted with equal velocities also cannot be realized in general for

cascade decays.

The expression for the transverse component of $\vec{P_3}$ can be worked out by a succession of Lorentz transformations and rotations. However, the expression is cumbersome and a rigorous derivation of the distribution of $\Delta P_\perp$ would be very difficult. We can get an estimate of the magnitudes of $\Delta P_\perp$ to be expected by taking the average values of the angles encountered: namely $\cos\theta' \sim .5$, etc. Then the magnitudes of $\Delta P_\perp$ to be expected will be of the order of

$$\tfrac{1}{2}P''(1+\frac{W_*{}'}{M_*}) + \frac{P'W_3{}''}{M_*}$$

Since the observed products come from two different decays, the distribution of α' will be very complicated and of little value.

H. Three-Body Decay With One Heavy Secondary

If one of the charged products of a decay scheme is very heavy, so that it takes a negligibly small fraction of the Q-value as kinetic energy in the center of mass system, the dynamics of various three-body decay schemes are particularly simple. This case is a usable approximation if one of the products is a proton and the others have masses no heavier than π-mesons. Of course, the results will then be inexact, but the statistical data from a limited number of observations is also very rough

and only general indications can be inferred from them.

As pointed out in section III-F, the probability distribution for P_1' for an uncoupled three-body decay becomes

$$\text{Prob}(P_1')dP_1' = 4\pi K P_1'^2 P_2' W_2' dP_1' \qquad (M_3 \text{ large})$$

If we investigate what this means in terms of the vector triangle in three-dimensional momentum space we find that the locus of (ξ, η, ζ) reduces to a sphere. This fact follows from the conservation of energy, which requires the magnitude of P_2' to be fixed, when P_1' is fixed, at a value corresponding to $T_2' = Q - T_1'$. Furthermore, introducing a weighting factor dependent only on angles has no effect on the distribution of P_1' since the integration over angles is independent of the magnitude of P_2', and thus independent of the magnitude of P_1'. In this case it might be possible to get correlations between the direction of emission of the secondaries, but the distribution of Q' and P_1' are unaffected.

If in addition to assuming that M_1 and M_2 are small compared to M_3 we also assume Q to be small we can calculate an approximate value for α:

$$\alpha \approx \frac{2M_3 - M_0}{M_0} + \frac{2}{\beta_0 M_0^2}[M_3 \beta_0 W_1' - (M_0 - M_3)P_1' \cos\theta_1' - M_0 P_2' \cos\theta_2']$$

where $\cos\theta_1'$ and $\cos\theta_2'$ are independently distributed uniformly between -1 and $+1$. Thus we get a distribution of α, for each value of W_1', centered about $\frac{2M_3(M_0 + W_1') - M_0^2}{M_0^2}$. However, we have assumed Q to be small compared to M_3

and therefore small compared to M_O. Therefore the central value of α will be near $\frac{2M_3(M_O+M_1)-M_O{}^2}{M_O{}^2}$. For β_O near 1 the width of the distribution will be smaller than this central value and the distribution will resemble quite closely the two-body decay α distribution when one secondary is heavy compared to the other.

IV. PRELIMINARY RESULTS ON NEUTRAL V-PARTICLE DECAYS

A. Introduction

During the year 1953 the 48" magnet cloud chamber
equipment has produced approximately 16,400 photographs.
The geometry of absorbers and cloud chambers has been
changed from time to time and many different minimum
coincidence requirements have been tried. No systematic
enumeration has been made of the number of penetrating
showers detected, nor of the average number of shower
particles present. Fig. 5 is a tabulation of the number
of V-particles detected by various coincidence require-
ments used with two different chamber geometries and
lead or copper absorbers. The data include only the runs
in which all three geiger counter trays had lead or
copper shielding completely around each counter to absorb
most knock-on electrons. The results suggest that the
extra density in lead makes it more efficient for the pro-
duction of V-particles. There is also an indication that
a larger fraction of the V-particles produced in lead
have measurable secondaries, i. e. have low momenta, but
the number of events involved is too small to make such
a conclusion definite.

During this year of operation a total of 360 neutral
V-particle decay events and 57 charged V-particle decay
events were observed in the 48" magnet cloud chambers.
Due to the limitation of available time, not all of these

Fig. 5. V^0 Decay Yields

Counters	Running time	Pictures per hour	$V^0!$ [*]	$V^0!$/hr.	V^0	V^0/hr.
Lead Absorbers With Four Chamber Geometry						
2-2-0+0-2-2	775	4.4	21	.027	64	.082
2-2-1+0-2-2	633	3.3	16	.025	57	.090
Lead Absorbers With Three Chamber Geometry						
2-2-1+0-2-2	572	2.6	21	.037	46	.080
Copper Absorbers With Four Chamber Geometry						
2-2-1+0-2-2	409	4.7	6	.015	32	.078
Copper Absorbers With Three Chamber Geometry						
2-2-1+0-3-2	749	3.1	19	.025	53	.071
2-2-1+0-2-2	542	3.9	16	.030	36	.066

This table summarizes the rate of detection of V^0 events with various counter requirements. The numbers 2-2-0 refer to the minimum number of counters in each tray which are required to fire simultaneously. The numbering sequence is from top to bottom. The three chamber geometry consists of the double-height chamber on top with two regular size chambers below.

---

[*]$V^0!$ refers to those decays in which the momenta of both secondaries can be measured. V^0 includes all identified V^0 decays.

cases have been analyzed and only a fraction of the in-
herent information has been extracted. The emphasis has
been placed on making accurate measurements on the best
cases. The definition of the best cases is not precisely
formulated, but it involves reasonable measurability on
the curvatures of both secondary tracks. The V^O decays
included in this summary were required to have an estimated
error of the Q-value less than one-third the calculated
Q-value. Such an a posteriori criterion introduces some
bias into the selection of cases, but it will not be sig-
nificant since no important conclusions will be drawn
from statistical data which are sensitive to this choice.

The problem of distinguishing Λ^O decays from θ^O decays
is an important one. The criterion adopted has led to
three classifications:

1. The positive product is clearly heavily ionizing
   and consistent with a proton.

2. The positive secondary is clearly lighter than a
   proton and its momentum and ionization are consis-
   tent with it being an L-meson.

3. The ionization of the positive secondary is indis-
   tinguishable from minimum but its momentum is so
   large that it could be a proton.

In considering Λ^O decays only cases in class 1 were
used. This criterion is likely to introduce some bias
favoring the proton being emitted backwards in the center

of mass system, and caution must be taken in interpreting
the data on the isotropy of emission of the secondaries.

In considering θ^0 decays, a number of class 3 parti-
cles were included in addition to the class 2 particles,
because the Q-value calculated assuming the decay to be
a Λ^0 decay was anomalously high. It is true that these
cases could be the high-Q Λ^0 decays which have been reported
previously, but considering them as θ^0-particles does not
alter any of the conclusions drawn from the data. Again
a bias is introduced favoring backward angles of emission
in the center of mass system for the positive secondary,
because slow positive secondaries are favored. It can
also be seen by examining a P_T vs. α diagram that for
$\beta_0 \sim .9$, the curve corresponding to a proton being emitted
forward in the center of mass system of a Λ^0 decay over-
laps part of the corresponding curve for a θ^0. Thus
in this region a number of cases will occur in which the
selection cannot be made on the basis of Q-value. Further-
more, when $\beta_0 \sim .9$, the ionization of a proton emitted for-
ward in the center of mass system is indistinguishable
from minimum when visual ionization estimates are made.

B. $\underline{\Lambda^0 \text{ Decays}}$

The question of the uniqueness of the Q-value for
the Λ^0 decay mode has long been a subject of contro-
versy.[3,4,6-8] Therefore, one of the first tasks to be

attacked with the new data was to calculate the Q-values for the best Λ^O decays. Naturally, the criterion of good measurability will tend to eliminate high-Q cases, on the average. Nevertheless, such a selection of cases should serve to distinguish between one or more unique Q-values and a distribution of calculated Q-values due to the presence of a three-body decay. The observed distribution would have no quantitative meaning until the bias were removed. Likewise the absence of cases with very high Q-values in the sample would not necessarily imply their nonexistence.

The Q-values of the Λ^O decays (class 1 only) were calculated from the measured values of P_+, P_- and θ, assuming the products to be a proton and a π-meson. The errors in the momenta were estimated and the corresponding error in the Q-value calculated. The cases for which $\Delta Q < Q/3$ were included in the histogram of Fig. 6, wherein the cases for which $\Delta Q \leqslant 5$ Mev contributed the shaded area. Each case was assigned a block of width 5 Mev, centered about the calculated Q-value, and height $\frac{Q^2}{100(\Delta Q)^2}$. The weighted mean and the weighted standard deviation of the best Λ^O decays ($\Delta Q \leqslant 5$) was computed analytically. The Gaussian curve drawn on Fig. 6 has the same area, mean, and standard deviation as this distribution. The weighting factor was $\frac{1}{(\Delta Q)^2}$ as prescribed by a least squares adjustment of the data.
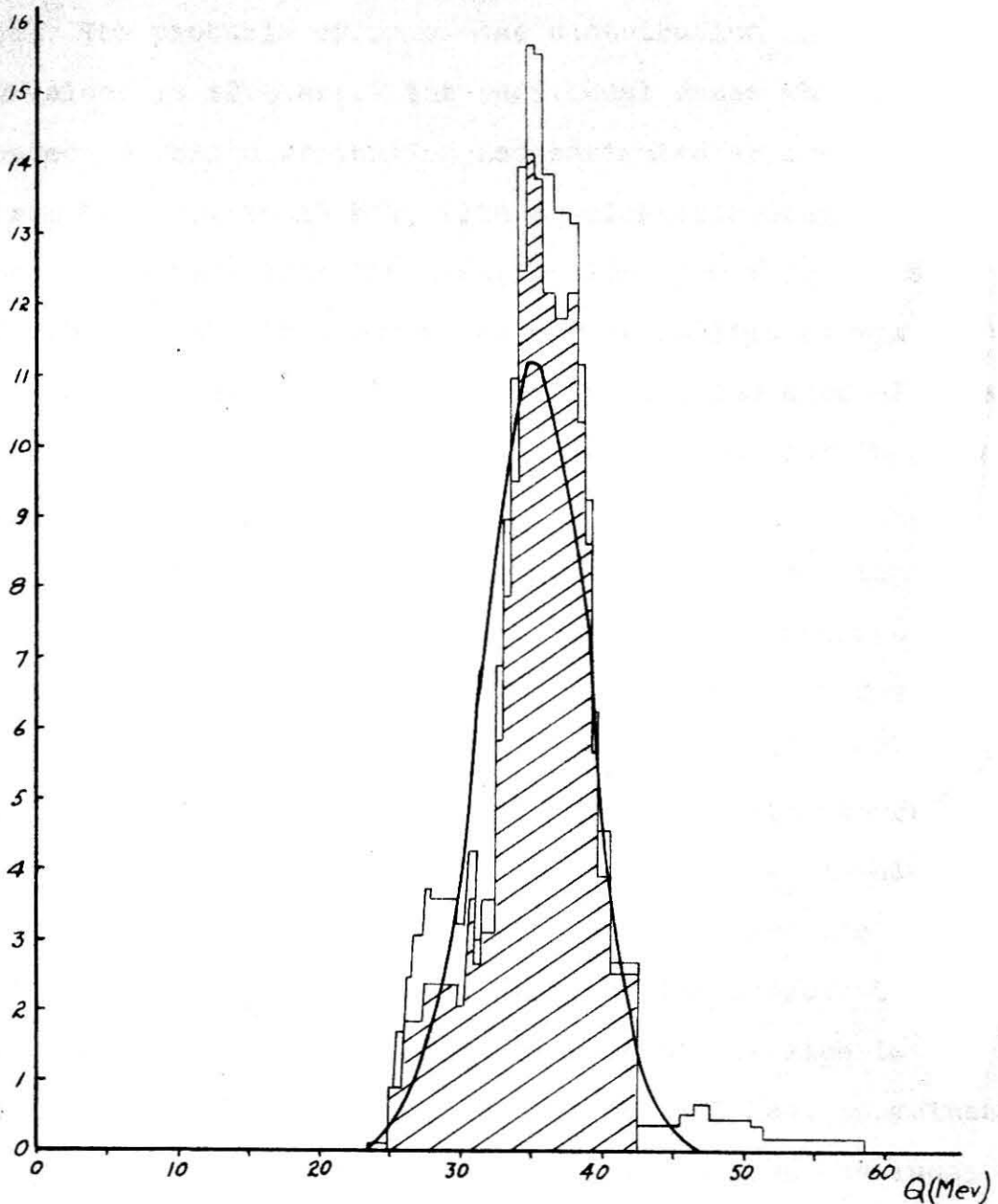
Fig. 6. Q-Values of Λ^0 Decays

Only cases with $\Delta Q < Q/3$ have been included in this histogram. Each case was assigned a block of width 5 Mev and height $\dfrac{Q^2}{100(\Delta Q)^2}$ centered about the calculated Q-value. The shaded portion is the contribution of 20 cases which have $\Delta Q \leqslant 5$ Mev.

The probable error of the distribution of the best Q-values is ±2.5 Mev. The individual cases which contributed to this distribution had estimated errors ranging from ±2.5 Mev to ±5 Mev, with a weighted average of ±3.3 Mev. The fact that the distribution of Q-values has a width less than the estimated errors implies firstly that the errors were slightly overestimated, and secondly that the distribution is indistinguishable from that due to a single two-body decay.

The presence of possible systematic errors in this Q-value determination has been discussed in section I-E. The only appreciable systematic error, which is due to the magnetic field calibration, has a magnitude of about ±.7%. The effect of this error on the Q-value through the proton momentum is negligible because $\frac{\partial Q}{\partial P_+}$ is always small. However, $\frac{\partial Q}{\partial P_-}$ is usually about .5, and the average value of P_- for these cases is about 150 Mev/c. Thus the estimated effect of such an error on the Q-value is to introduce a systematic error of about ±.5 Mev. Combining this with the statistical error of ±.5 Mev we conclude:

$$\Lambda^\circ \rightarrow P^+ + \pi^- + (34.8 \pm 1)\text{Mev}$$

An examination of the histogram in Fig. 6 reveals that inclusion of all cases for which $\Delta Q < Q/3$ does not change the conclusion that the data are consistent with a single two-body decay.

The existence of a two-body decay with a Q-value,

calculated assuming $(\Lambda^0 \rightarrow P^+ + \pi^-)$, near 35 Mev seems well established by these data. Other Q-values, particularly very high ones, cannot be excluded due to the small sample and selection bias. However, it can be stated that such cases probably do not occur at low energy more frequently than once for every ten of the 35 Mev cases.

Photographs of Λ^0 decays in a regular size chamber and the double-height chamber are reproduced in Figs. 7 and 8, respectively. These demonstrate the fact that the cloud chambers are designed so that the camera can photograph tracks within .5 cm. of the top and bottom walls. Thus a V-particle can be produced in the walls, or in the absorber lying on the walls, and have its decay observed in the chamber gas after a flight of only a few centimeters. Thus the decay of very slow cases can still be observed in the chamber. Furthermore, the illuminated region of the chambers is quite deep ($\sim$20 cm.) so that particles emitted at large angles with the vertical direction can also be observed frequently. These facts account for the large number of low energy Λ^0-particles observed and the accuracy of the resultant data.

A search has been made in all of these photographs for possible origins for the Λ^0's. When such an origin is located accurately, the coplanarity angle δ and the transverse momentum unbalance ΔP_T can be computed. In most of these cases the limiting factor in the determin-
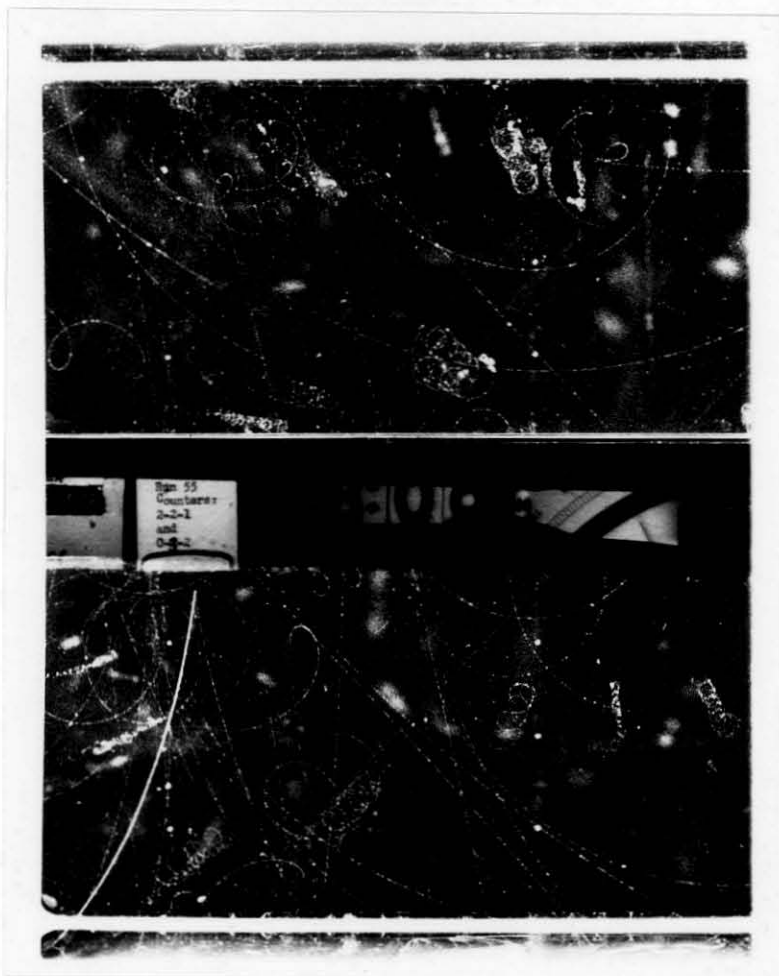
Fig. 7. Photograph 14979 (Λ^o Decay)

The Λ^o decay occurred at the left in the bottom cloud chamber. The momentum of the positive secondary is unusually low (110 ± 20 Mev/c). There is no clear origin in the copper plate between the chambers, but there is evidence of nuclear interactions. The Q-value is calculated to be 35.5 ± 2.5 Mev.
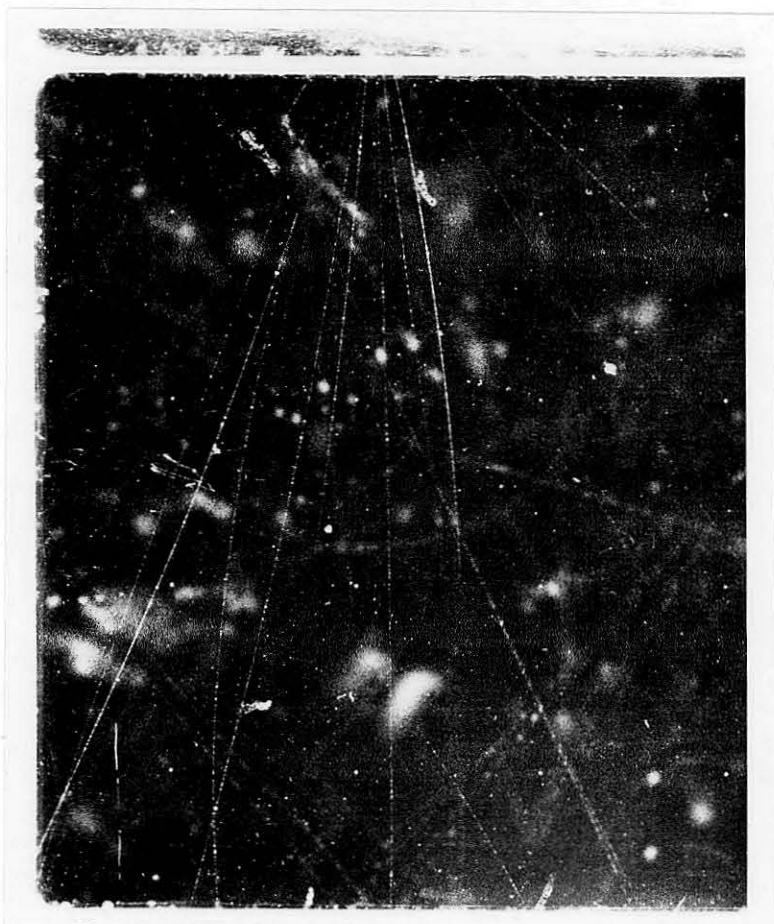
Fig. 8. Photograph 23023 (Λ° Decay)

The narrow angle Λ° decay occurred at the left of the main shower traversing the double-height cloud chamber. The long tracks available make this a well measurable case despite the high primary momentum (763 ± 35 Mev/c). The plane of decay of the Λ° includes the excellent origin and transverse momentum balances within the experimental uncertainties. The Q-value is calculated to be 36 ± 4 Mev.

ation of these quantities was the accuracy of location of the origin. However, an upper limit on the magnitude of the momentum of a possible neutral third secondary can be estimated by observing the prevailing magnitudes of ΔP_T and $P_O \delta$. For a unique value of $P_n{}'$, the distribution of $\sqrt{(\Delta P_T)^2 + (P_O \delta)^2}$ should be peaked near $P_n{}'$. Thus, the radius of a circle which encloses most of the Λ^O points on the ΔP_T vs. $P_O \delta$ plot of Fig. 9 should be an estimate of the maximum value of $P_n{}'$ which could be present. The maximum value of 70 Mev/c estimated from Fig. 9 is probably high since most of the values of ΔP_T and $P_O \delta$ plotted in Fig. 9 can be explained by the experimental inaccuracy in locating the origin. The only origins that were discarded as being obviously inappropriate were ones for which the unbalanced momentum would have been many times this value.

C. θ^O Decays

Two photographs of θ^O decays are reproduced in Figs. 10 and 11. The Q-values, calculated assuming two π-meson secondaries, for all cases in class 2 (light positive secondary), as well as for those in class 3 which cannot be ordinary Λ^O decays, have been plotted in Fig. 12. Again, the momenta of the secondaries and the angle between them were used to calculate the Q-value. The data represent a large range of Q-values and therefore it is desirable to indicate the significance of the percentage
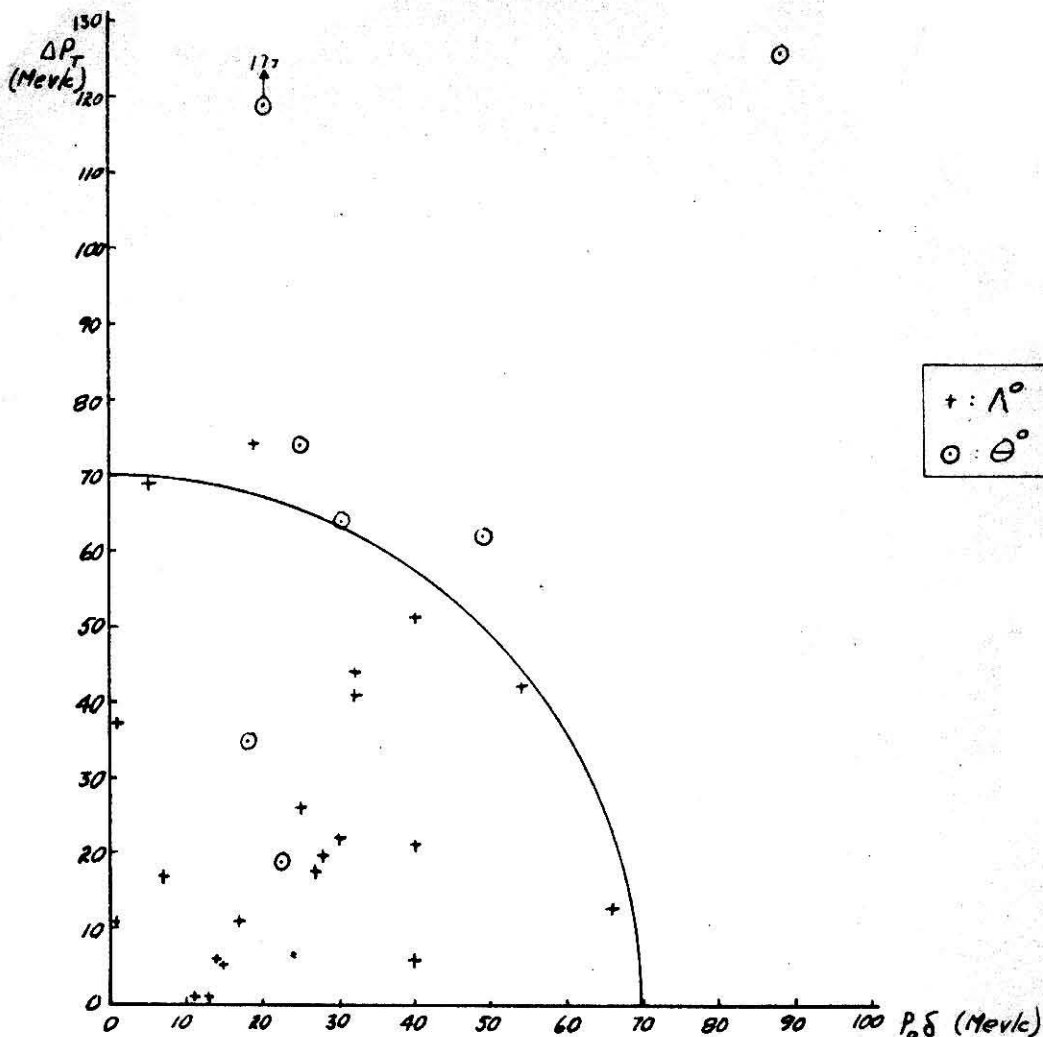
Fig. 9. ΔP_T vs. $P_o\delta$ for Λ^o's and θ^o's.

Most of the Λ^o values of ΔP_T and $P_o\delta$ are consistent with the estimated experimental uncertainties. A circle of radius 70 Mev/c encloses most of the Λ^o points indicating that these data cannot rule out a possible neutral third product whose momentum is usually less than this number. Many θ^o points lie well outside this circle, but there are not enough cases of θ^o decays to draw any conclusions.
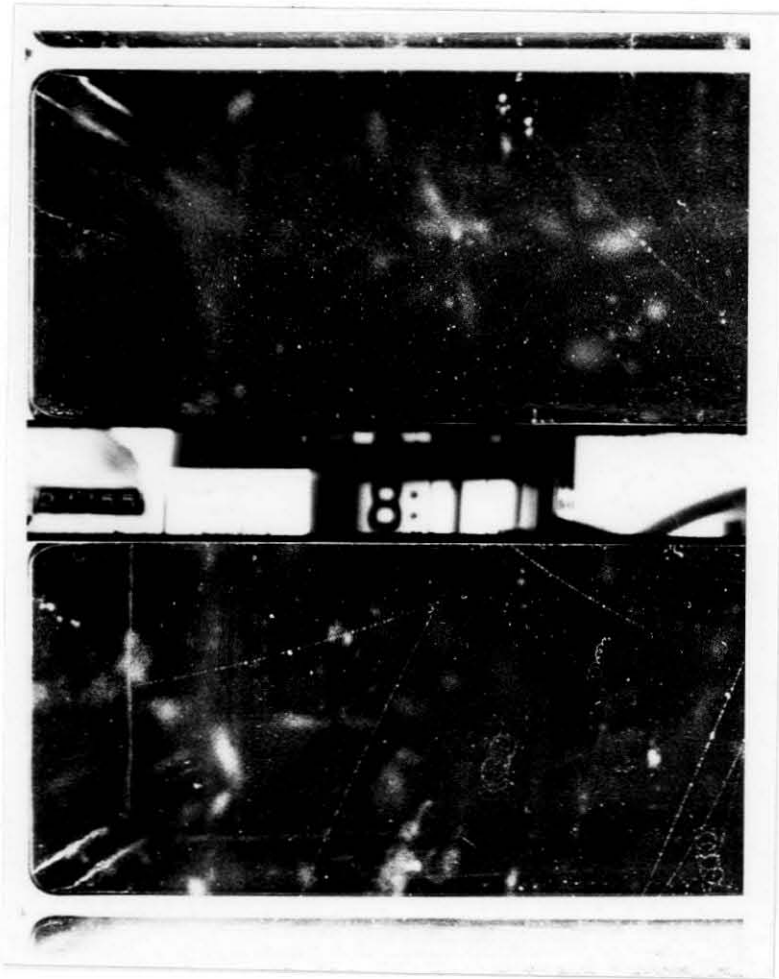
Fig. 10. Photograph 9630 (θ^O Decay)

This photograph illustrates a θ^O decay observed in the second chamber of the four chamber geometry. The line of flight of the θ^O (assuming a two-body decay) comes forward in the chamber, so that the origin may lie behind the top chamber. The positive momentum of 265 ± 19 Mev/c makes its ionization inconsistent with that of a κ-meson. The Q-value, calculated assuming two π-mesons as secondaries, is 186 ± 38 Mev.
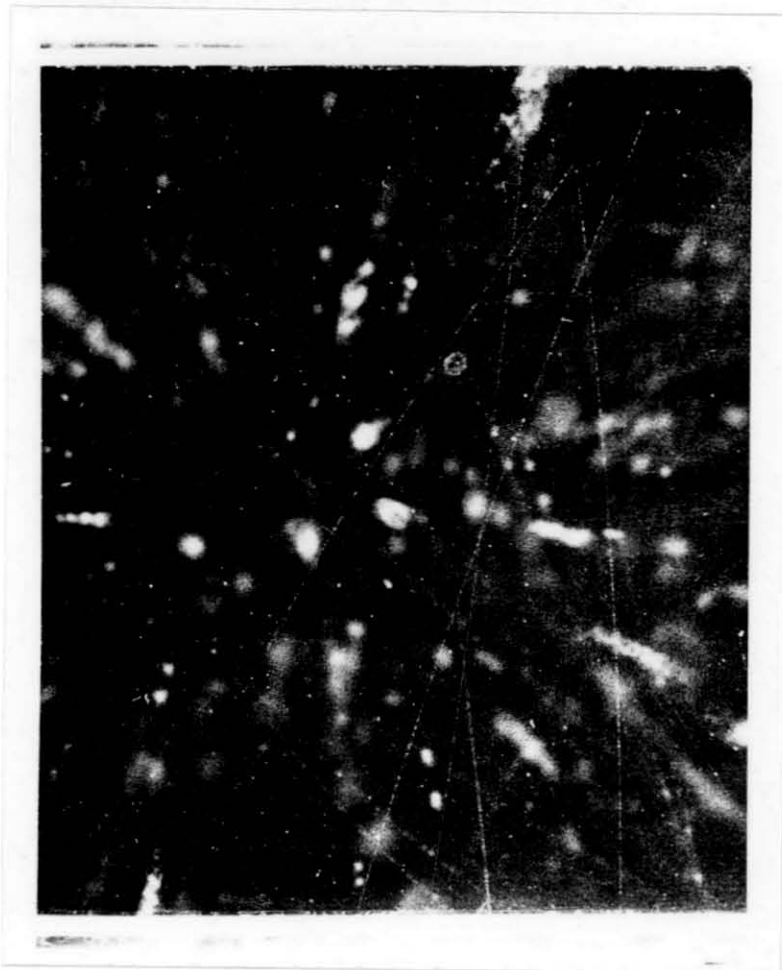
Fig. 11. Photograph 22332 (θ^0 Decay)

This is the best example of a θ^0 decay observed with the 48" magnet cloud chambers. The positive secondary appears to undergo a single scattering or a π-μ decay (deflection $\sim .7^0$) at a point one-third of its length from the apex. The Q-value is calculated to be 215 ± 17 Mev.

Fig. 12. Q-Values of θ^0 Decays
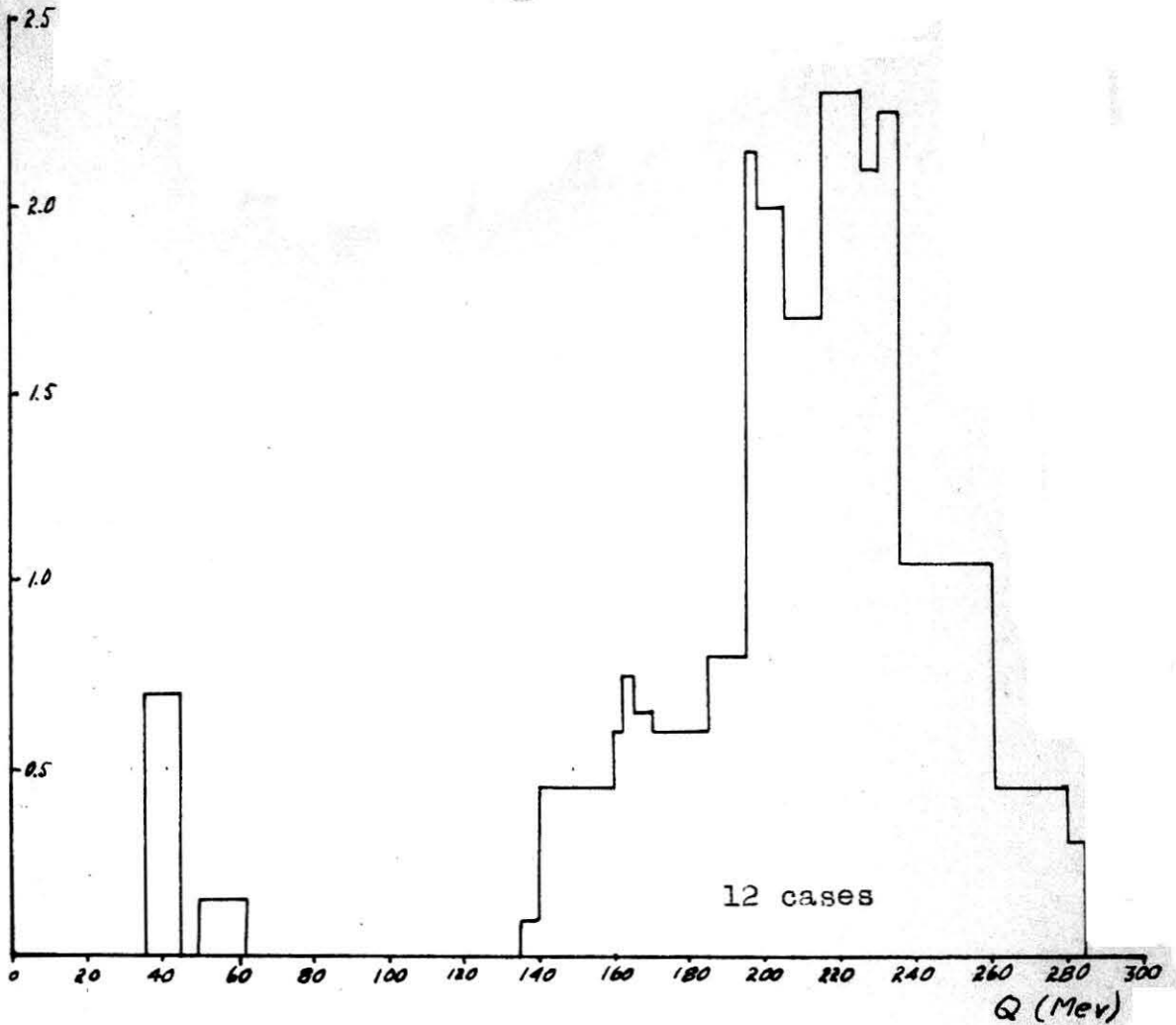
Only cases with $\Delta Q < Q/3$ have been included in this histogram. Each case was assigned a block of width $Q/5$ and height $\dfrac{Q^2}{100(\Delta Q)^2}$ centered about the calculated Q-value. The statistics are very poor since most of the peak is contributed by one case (see Fig. 11). The two cases near 40 Mev are "anomalous θ^0" decays described in Section IV-D.

error rather than the absolute error in each case. There-
fore the cases were assigned a block of width $= Q/5$ and a
height $\dfrac{Q^2}{100(\Delta Q)^2}$.

At once it is clear from Fig. 12 that the quality of
these data is not comparable to the Λ^0 data. The explana-
tion for this fact lies in the observed phenomenon that
the slowest θ^0-particles are observed at much higher
momentum than the slow Λ^0-particles.

The distribution of Q-values near 200 Mev is consis-
tent with a unique two-body decay, although these data
alone are not good enough to establish such a conclu-
sion.[3,4] However, there exists an excellent case, no.
19143B, whose calculated Q-value is 41 ± 5 Mev. This case
forms the basis of the discussion of "anomalous θ^0" decays
in section IV-D.

The possible origins have been located and Fig. 9
presents the resulting values of ΔP_T and $P_0 \delta$. The number
of cases is too small to draw any conclusions from these
data. The only indications observed subjectively are
that the origins for the θ^0-particles are not as clearly
located, nor do the values of ΔP_T and $P_0 \delta$ fall within
the estimated errors as often as for the Λ^0's. The
explanation for these observations, if true, may be con-
nected with the high average primary momentum: namely,
the particles travel farther before decaying and thus
are not clearly associated with a single origin.

D. "Anomalous θ^O" Decays[*]

1. Introduction

It has been recognized for some time by many laboratories that decay events exist which cannot be explained by the $\Lambda^O(P,\pi,35 \text{ Mev})$ or $\theta^O[\pi,L,214(\pi,\pi)]$ decay modes. (1,3,4,8-12) One of these anomalous modes is the so-called high-Q Λ^O-particle. Another is the $V_3^O(L^+,\kappa^-)$ mode suggested by one photograph from the 18" magnet cloud chambers,(8) which could also be a charged V decay with an anomalously large energy release. The 48" magnet cloud chambers have to date furnished no evidence for either of these decay modes. However, a case of a decay into two light secondaries with a very small energy release has been observed. Similar cases have been observed in other laboratories, but many of these could have been explained by the V_3^O decay scheme. The following discussion will present in detail the data from the three best cases observed in the three Caltech magnet cloud chambers. Four more cases will be added to the tabulated data, and an attempt will be made to enumerate some of the possible interpretations.

2. Photograph 8796 (18" Magnet)

Fig. 13 is a reproduction of the first of these

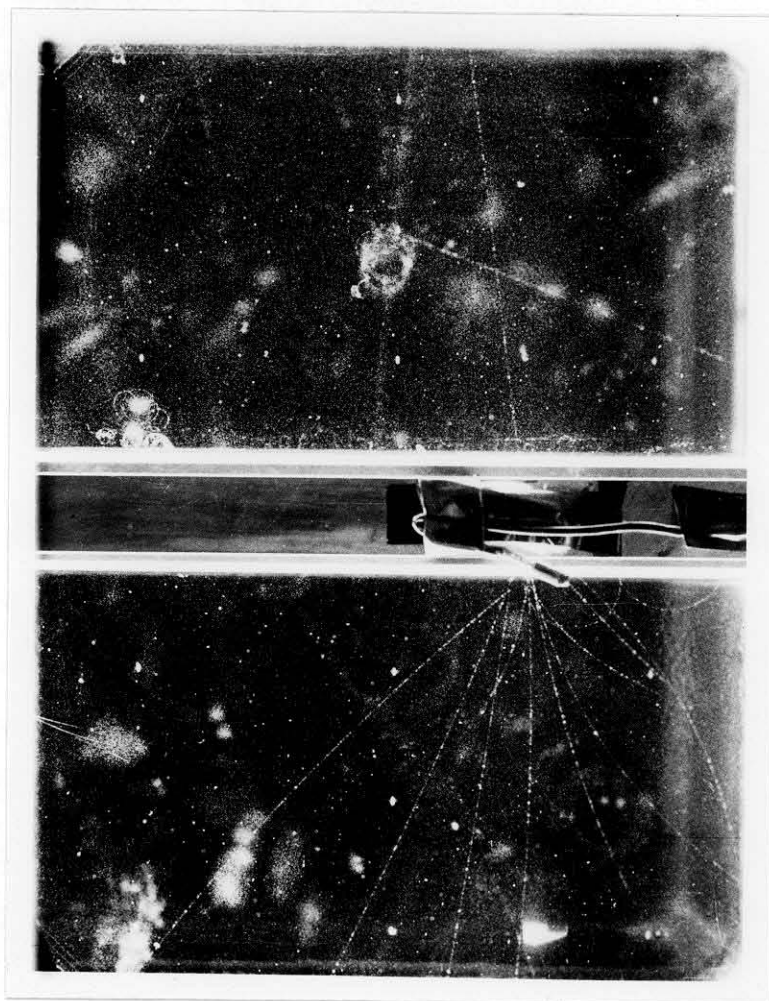[*]The following discussion is essentially that published in reference number 14.

Fig. 13. Photograph 8796 ("Anomalous θ^0" Decay)
(18" magnet)

The V^0 decay is observed just below the lead plate.
The V^0-particle probably originated at the interaction in
the lead plate. A positive particle corresponds to a
clockwise curvature.

unusual V^O decays observed in this laboratory.[11] The V^O-particle decayed in the lower chamber and was undoubtedly produced in the interaction in the lead plate between the two chambers. The energy release calculated assuming the products to be two π-mesons is 116 ± 30 Mev. The momentum of the positive particle (curved clockwise) would have to be doubled in order to make the calculated Q-value of this event 214 Mev, or to make it consistent with the decay of a Λ^O-particle with a Q-value of 35 Mev. The plane of the decay products contains the interaction in the lead plate within the large errors of measurement introduced by the shortness of the line of flight of the unstable particle. Also the components of the momenta perpendicular to the assumed line of flight of the V^O-particle balance within experimental accuracy. This statement would not be true if the positive momentum were doubled.

3. Photograph 12590 (21" Magnet)

    Fig. 14 shows the decay of a V^O-particle into two light secondaries. On the original film the individual droplets are clearly resolved along all tracks in the chamber.[13] Therefore the relative ionization of the V-particle secondaries and comparison tracks can be determined. If the identity and momenta of the particles producing the comparison tracks are known, then through

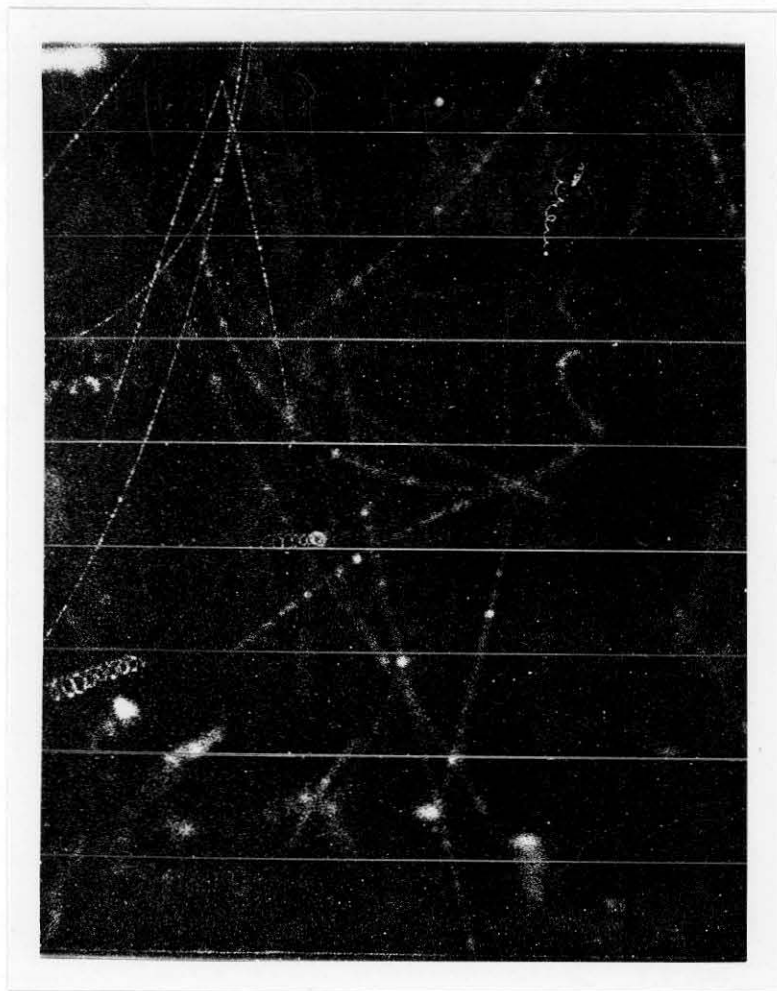Fig. 14. Photograph 12590 ("Anomalous θ^O" Decay)
(21" magnet)

The V^O decay is in the upper left corner and the
secondaries both leave the chamber through the rear wall.
Individual droplets can be counted on the original photo-
graph permitting a comparison of the ionizations of the
secondaries and the two curved electron tracks. A nega-
tive particle corresponds to a clockwise curvature.

the application of a theoretical expression for the dependence of ionization on velocity, the specific ionization of the V-particle secondaries can be determined. In the present case the two highly curved comparison tracks are identified as electrons, and the resulting values for the ionizations of the positive and negative secondaries of the V-particle are 1.4 ± 0.2 and 1.3 ± 0.2, respectively. These values are probably too high, since a preliminary study of the ionization of electrons in the velocity range of the comparison tracks has indicated the actual ionization to be somewhat less than that given by the theoretical formula.

The measured momentum of the negative secondary is 249 ± 12 Mev/c and if it is assumed to be a π or μ-meson, its specific ionization is 1.1. Using this track as a comparison track the specific ionization of the positive secondary is 1.2 ± 0.2. The momentum of the positive track is 493 ± 33 Mev/c. If it is assumed to be a κ-meson its specific ionization is 1.6. Therefore, the present measurements make unlikely the possibility that the secondaries are a π or μ-meson and a κ-meson, although the possibility that either or both might be electrons cannot be excluded from ionization measurements.

The energy release calculated assuming the secondaries to be two π-mesons is 79 ± 10 M_ev. The short straight track and the longer electron track appear to intersect

in the lead above the chamber, although the exact inter-
section is uncertain due to the large possible multiple
scattering of the electron. This possible origin lies
in the plane of decay of the V^0-particle and the compon-
ents of momentum transverse to the assumed line of flight
of the V^0-particle balance within experimental error.

4. Photograph 19143 (48" Magnet)

    Fig. 15 shows two decay events which occurred at
points A and B in the large upper cloud chamber of the
48" magnet. The decay at point A is consistent with the
usual θ^0 decay scheme. Its energy release, assuming the
products to be two π-mesons, is 238 ± 30 Mev.

    The decay which appears at point B in this photograph
has a Q-value of 41 ± 5 Mev, calculated assuming two π-
mesons as the only decay products. If this event actually
represents a two-body decay, momentum balance requires
that the point of production of the parent particle lie
on the extension of the line BP which lies within the
illuminated region of the chamber. Extensions of the
lines of flight of all charged particles in the chamber
other than electrons and heavily ionizing tracks locate
two intersections in the lead plate above the chambers at
O_1 and O_2. In addition there are two more nuclear inter-
actions at O_3 and O_4 in the upper chamber wall from which
only heavily ionizing tracks emanate. Whereas event A

shows good coplanarity and transverse momentum balance if O_2 is assumed to be its origin, it is clear for event B that there is no evidence for any interaction along the extension BP. Furthermore, the locations of the inter- actions above the chamber indicate that the penetrating shower was probably initiated by a single primary inter- acting at O_1, with secondaries producing further inter- actions at O_2, O_3, and O_4. It seems quite improbable that a secondary from one of these events was emitted at near- ly 90° to the primary direction, interacted at the right of the lead plate and emitted an energetic unstable par- ticle in a backward direction along the line PB, and fur- thermore produced no charged secondaries which entered the chambers.

We thus conclude that this event is probably not a two-body decay. The possibility that it is a three-body decay will now be discussed.

If one assumes the origin of production of the par- ent particle to be any of the four observed interactions, the component of momentum of the neutral secondary perpen- dicular to the primary line of flight lies in the range 170 ± 20 Mev/c to 210 ± 25 Mev/c. This information, to- gether with the assumption of the mass of the neutral secondary, determines a lower limit to the Q-value of the three-body decay.

If one assumes the neutral secondary to be a π^o-

meson, by analogy with the charged τ decay scheme, the lower limit on the Q-value is 165 ± 20 Mev. The Q-value of the charged τ-meson is known to be 75 ± 1 Mev, and thus the interpretation of this event as a $\tau^0(\pi^0,\pi^+,\pi^-,\sim 80)$ decay is inconsistent with the assumption that the particle originated in one of the four observed interactions.

5. Summary of Cases

Fig. 16 tabulates the important data from the events described and a few others. The ionization of all tracks except those of #12590 were estimated visually.

Three of the four cases that have been added to this tabulation have no clear origin for the parent particle. Nevertheless, the estimated ionizations and the orientations make such possible alternatives as the decay of a κ-meson unlikely. Some of these events could also be interpreted as the decay of a neutral particle into a π or μ-meson and a κ-meson. However, no simplification would result from such an assumption since the best cases cannot be so interpreted.

6. Discussion

It is tempting to interpret the cases which have a very low Q-value as representing the decay of a neutral τ-meson into three π-mesons. However, it has been shown that such an interpretation is very unlikely for at least

Fig. 16. Data on "Anomalous θ°" Decays

Event	Secondary	Momentum	Specific Ionization	Mass	Angle Between Secondaries	Q(π,π)
8796 (18")	+	570±130	1 - 1.7	<1200Me	44°	116±30
	-	120±5	1.5- 3	220-420		
56337 (18")	+	240±65	1 - 1.7	<600	63°	148±30
	-	390±30	1 - 1.7	<830		
59824 (18")	+	124±10	1 - 2	<310	61°	96±16
	-	365±55	1 - 1.7	<780		
12590 (21")	+	493±33	1.4±1.2*	840±150*	34°	79±10
	-	249±12	1.3±1.2*	385±130*		
15329 (48")†	+	940±100	1 - 1.7	<2000	8°	45 +25 -12
	-	1420±300	1 - 2	<3500		
19143A (48")	+	375±30	1 - 2	<970	46°	238±30
	-	820±70	1 - 1.7	<1700		
19143B (48")	+	260±20	1 - 2	<640	40°	41±5
	-	87±4.5	1.5- 3	160-300		
20411 (48")††	+	880±150	1 - 1.7	<1800	15°	57±15
	-	525±150	1 - 2	<1300		

*These values are calculated assuming the dubious theoretical electron ionization and are probably too high.

†This case is included here because $Q(p,\pi)$ would be 343±80.

††The positive secondary traverses a 2" lead plate with no apparent increase in ionization. Also $Q(p,\pi)$ would be 104±50.

one such case (19143B). In addition there are a number
of cases whose two-body Q-values are already too high
to be interpreted as such a τ^O decay.

If one wishes to retain the simplifying assumption
that most of these cases are decays of the same particle,
a scheme with a much higher energy release is required.
One possible decay scheme which satisfies this requirement
is an alternate mode of decay of the θ^O-particle into
$\pi+\mu+\nu$. The computed energy release for this decay is
about 244 Mev.

Calculation of the minimum Q-value assuming
$\theta^O \rightarrow \pi^+ + \mu^- + \nu$ for case 19143B yields 245 ± 30 Mev. Thus
such an hypothesis would explain all of these unusual
cases. It should be pointed out, however, that this
decay scheme is certainly not a unique one. For example,
another decay scheme which can explain all of these cases
is θ^O or $\tau^O \rightarrow \pi^O + \mu^+ + \mu^- + (\sim 148$ Mev). Both of these
hypotheses are so broad that they can explain almost any
individual event of the type considered here. To confirm
or to disprove either of them would require a large amount
of accurate data on these rare events.

It is possible that the $\theta^O(\pi,\pi)$ decays having Q-
values near 214 Mev represent a part of the same three-
body decay distribution. However, if this were the case
it is unlikely that the observed $Q(\pi,\pi)$-value distribution
should be as sharply peaked as present experimental measure-
ments appear to indicate.

7. Summary

There is evidence for the existence of a neutral particle which decays into two charged L-mesons which cannot be explained by the scheme $\theta^O \rightarrow \pi^+ + \pi^- + (214 \text{ Mev})$. If only two-body decays are considered, at least two different new particles have to be postulated with $Q(\pi,\pi)$ near 41 Mev and 90 Mev respectively, and under this assumption a question as to the point of production in at least one case still remains. Not all of these cases can be explained by the decay of a neutral τ-meson into three π-mesons. Hence a decay scheme with a higher energy release is indicated. One scheme which might explain these cases in terms of an alternate mode of decay of a known particle is $\theta \rightarrow \pi^{\pm} + \mu^{\mp} + \nu + (\sim 244 \text{ Mev})$. Of course, many other decay schemes might be postulated, but there is no direct experimental evidence for any particular one of these.

BIBLIOGRAPHY

1. Armenteros, Barker, Butler, Cachon; Phil. Mag. 42, 1113, (1951)

2. Podalanski, Armenteros; Phil. Mag. 45, 13, (1954)

3. Thompson, Buskirk, Etter, Karzmark, Rediker; Phys. Rev. 90, 1122(L) (1953)

4. Thompson, Buskirk, Cohn, Karzmark, Rediker; Report B-2 at Bagneres Conference (1953)

5. Brueckner, Thompson; Phys. Rev. 87, 390 (1952)

6. Armenteros, Barker, Butler, Cachon, Chapman; Nature. Lond. 167, 501 (1951)

7. Armenteros; Report A-8 at Bagneres Conference (1953)

8. Leighton, Wanlass, Anderson; Phys. Rev. 89, 148 (1953)

9. Ballam, Harris, Hodson, Rau, Reynolds, Treiman, Vidale; Phys. Rev. 91, 1019(L) (1953)

10. Reynolds; Report B-5 at Bagneres Conference (1953)

11. Leighton, Wanlass, Alford; Phys. Rev. 83, 843(L) (1951)

12. Barker; Report B-3 at Bagneres Conference (1953)

13. Cowan; Phys. Rev., April (1954) (in press)

14. van Lint, Anderson, Cowan, Leighton, York; Phys. Rev. (in press)